Manifestation of ocular-muscle EMG contamination in human intracranial recordings

Christopher K. Kovach [a,c,d,*], Naotsugu Tsuchiya [b,c], Hiroto Kawasaki [a], Hiroyuki Oya [a], Mathew A. Howard III [a], Ralph Adolphs [a,b,d]

[a] Department of Neurosurgery, The University of Iowa College of Medicine, Iowa City, IA, USA
[b] Division of Humanities and Social Sciences, California Institute of Technology, Pasadena, CA, USA
[c] Brain Science Institute, Tamagawa University, Tokyo, Japan
[d] Division of Biology, California Institute of Technology, Pasadena, CA, USA

ARTICLE INFO

ABSTRACT

It is widely assumed that intracranial recordings from the brain are only minimally affected by contamination due to ocular-muscle electromyogram (oEMG). Here we show that this is not always the case. In intracranial recordings from five surgical epilepsy patients we observed that eye movements caused a transient biphasic potential at the onset of a saccade, resembling the saccadic spike potential commonly seen in scalp EEG, accompanied by an increase in broadband power between 20 and 200 Hz. Using concurrently recorded eye movements and high-density intracranial EEG (iEEG) we developed a detailed overview of the spatial distribution and temporal characteristics of the saccade-related oculomotor signal within recordings from ventral, medial and lateral temporal cortex. The occurrence of the saccadic spike was not explained solely by reference contact location, and was observed near the temporal pole for small (<2 deg) amplitude saccades and over a broad area for larger saccades. We further examined the influence of saccade-related oEMG contamination on measurements of spectral power and interchannel coherence. Contamination manifested in both spectral power and coherence measurements, in particular, over the anterior half of the ventral and medial temporal lobe. Next, we compared methods for removing the contaminating signal and found that nearest-neighbor bipolar re-referencing and ICA filtering were effective for suppressing oEMG at locations far from the orbits, but tended to leave some residual contamination at the temporal pole. Finally, we show that genuine cortical broadband gamma responses observed in averaged data from ventral temporal cortex can bear a striking similarity in time course and band-width to oEMG contamination recorded at more anterior locations. We conclude that eye movement-related contamination should be ruled out when reporting high gamma responses in human intracranial recordings, especially those obtained near anterior and medial temporal lobe.

© 2010 Elsevier Inc. All rights reserved.

Introduction

Cell-population level signals are important in the study of brain physiology because they index activity across many scales of time and anatomy, can be measured non-invasively at the scalp as well as intracranially and can reveal large-scale interactions in the brain (Engel et al., 2005; Lachaux et al., 2006). Recording of such signals has become particularly important in the diagnosis and clinical evaluation of a number of disorders, such as epilepsy. Yet despite the clinical and experimental usefulness of such signals, determining their physiological origin with sufficient detail and certainty to address experimental questions (the so-called inverse problem) remains a significant challenge, given the multitude of possible neural and extra-neural bioelectric sources (Baillet et al., 2001). A sobering reminder that the inverse problem extends well beyond the discrimination of cortical

sources is the recent observation that signals generated by the eye muscles during saccades can be mistaken for scalp-EEG activity in the gamma band (Reva and Aftanas, 2004; Trujillo et al., 2005; Yuval-Greenberg et al., 2008). The EMG signal arising from ocular muscle (oEMG), which commonly manifests as the "saccadic-spike potential" in scalp recordings (Becker et al., 1972), can be misinterpreted as a cortical gamma-band responses in averages of spectral power (Yuval-Greenberg et al., 2008). The problem is worsened by the fact that eye movements are correlated with many cognitive processes and cannot be fully controlled through instructed fixation (Engbert and Kliegl, 2002). The failure to appreciate the contribution of saccade-related oEMG has cast some doubt on a substantial part of the literature on gamma-band EEG responses in attentional and perceptual processing (Fries et al., 2008). Such limitations of physiological specificity are overcome using invasive recordings from the brain in patients for which such recordings are clinically justified. Intracranial recordings provide an increasingly important complement to other methods of studying the functional organization of the human brain (Jerbi et al., 2009b). Direct recordings are typically obtained from subdurally implanted electrode strips and

grids (ECoG) or from penetrating depth electrodes implanted in the brain parenchyma. In contrast to scalp recordings, intracranial recordings have been regarded as comparatively immune to oEMG contamination (Fries et al., 2008; Meador et al., 2002; Yuval-Greenberg et al., 2008). This assumption stems from the fact that they are obtained near the generating cortical sources and from the differing conductive properties of intra- and extra-cranial compartments.

Recent work has placed some qualifications on this assumption. In particular Jerbi et al. describe saccadic spikes in data from closely spaced bipolar stereotactic EEG (sEEG) at the immediate apex of the temporal pole (Jerbi et al., 2009a). The authors, however, found no contamination at other more posterior recording locations and therefore concluded that oEMG does not pose a significant problem for closely spaced bipolar sEEG recordings of the type examined, except in a very limited region near the temporal pole. Their finding leaves open the possibility that other recording methods and referencing schemes might be more severely affected. In particular, their study did not address how the signal might manifest in recordings referenced to a common intracranial or extracranial contact or to a global average, as is frequently used in human electrocorticography (ECoG). Two other studies have identified more widely distributed muscle artifacts in common-reference ECoG, including low frequency contamination related to blinks (Ball et al., 2009), and high frequency contamination arising from facial muscle EMG activity during seizures and mastication (Otsubo et al., 2008). These studies establish that eye-movement and motor contamination can affect ECoG under some circumstances, and that the presence of muscle artifacts in intracranial recordings cannot be discounted. The recognized potential for saccade-related oEMG to produce misleading results in scalp EEG makes the thorough investigation of the presence and distribution of oEMG in intracranial recordings especially important, as well as the identification of measures for suppressing or ruling out contamination.

Here we addressed this open issue, using data from epilepsy patients implanted with high-density cortical surface and depth electrodes. We provide a detailed map of the presence and distribution of saccade related oEMG signals near ventral and lateral temporal cortex. We found that under some circumstances intracranial recordings can be greatly affected by eye movement contamination even at substantial distance from the temporal pole. In particular, we found that the intracranial manifestation of the saccadic spike occurs at a similar scale and magnitude as at the scalp. In the present case, we observed that the signal is greatest near temporal pole, in the vicinity of the affected region described by Jerbi and colleagues, but that in common-reference data it is also detected many centimeters from the poles, affecting in particular recordings from anterior ventral and medial temporal lobe. In power spectral averages the signal may resemble visually induced cortical gamma-band responses in both time course and spectral distribution. We observe the effect of the signal in both power spectral measurements and in interchannel coherence. We consider the importance of reference location in these observations. Finally, we evaluated the effectiveness of two forms of spatial filtering, independent component analysis (ICA) filtering and nearest-neighbor bipolar rereferencing. Bipolar rereferencing is often easy to implement offline and is supported by the finding of Jerbi et al, while the application of ICA in the removal of muscle artifact in scalp based recordings has shown recent promise (Keren et al., 2010; McMenamin et al., 2010). We found that both methods reduced the extent of contamination, with ICA performing somewhat more favorably than bipolar rereferencing alone. Applying these methodological considerations allowed us to clearly separate genuine cortical activity in the gamma range from the eye movement-related artifact, and to demonstrate similarities and differences in their time course and spectral characteristics. Based on these observations we formulate a set of recommendations on how to avoid mistaking oEMG for cortical gamma band activity in intracranial recordings.

Materials and methods

Subjects and recording

Intracranial recordings were obtained from surgically implanted electrodes in 6 epilepsy patients (2 women; mean age 32, range 21–38) during chronic monitoring for cortical epileptogenesis (Howard et al., 2000; Tsuchiya et al., 2008). One subject was excluded from subsequent analysis after it was learned that he was amblyopic and therefore did not exhibit normal eye movements in both eyes. All subjects provided informed consent for their participation in research, and procedures were approved by the University of Iowa Hospitals and Clinics Internal Review Board.

We recorded simultaneously 128 channels from subdurally implanted ECoG grids, strip electrodes and multicontact penetrating depth electrodes (Howard et al., 1996) (Ad-Tech Medical Instrument Corporation, WI, USA). Grids (8×8 or 8×12) covered the lateral temporal surface, while 4-contact strip and 16-contact (8×2) grid electrodes were inserted below the ventral temporal surface. Depth electrodes were targeted to left and right amygdalae, and left or right Heschl's gyrus, and data were obtained from 4 contacts. Subdural strip and grid contacts were 4 mm platinum-iridium discs embedded in a plastic matrix, with 2.3 mm exposed diameter. Depth electrodes were platinum-iridium cylinders, 2 mm in length surrounding a flexible tecoflex-polyurethane shaft, 1.25 mm in diameter. Electrode impedance ranged between 5 k and 20 k Ohm. Inter-electrode distance was 5 mm for grids and 10 mm for strip and depth contacts. In each case data were recorded referenced to an extracranial channel implanted under the galea near the cranial vertex. Data were recorded continuously at a sampling rate of 24.4 KHz, filtered from 1.6 Hz to 1000 Hz and decimated to 2034.5 Hz before storage. All acquisition and online processing was carried out by dedicated research equipment (RX5 and Medusa Preamp, Tucker Davis Technologies, Alachua, FL), which recorded in parallel with clinical recording equipment. Data acquired continuously during experimental blocks were stored to hard disk for later processing.

Stimulus presentation

Stimuli were presented on a 17-in. LCD monitor (ViewSonic VX922, ViewSonic Corp., Walnut, CA) at 1024×768 resolution and a distance between 63 and 76 cm. Stimuli were generated on a Dell Optiplex GX280 PC computer (Dell Inc., Austin, Texas) using the software Presentation (Neurobehavioral Systems, Albany, CA). Event signals generated by the parallel port of the stimulus presenting PC indicated trial onsets and button presses and were recorded as analog inputs to the eye tracking system and digital inputs in the signal acquisition system. Event signals were used for offline alignment of eye movement and electrophysiological data after accounting for a 25-ms (3 video frames) processing lag in the output of the eyetracker and a measured 23 ms (± 0.4 ms) lag between the event signal and the first video frame containing the stimulus.

Task

All patients engaged in a task requiring overt visual search for upright and inverted faces (Fig. 1). The task was divided into blocks of 72 trials. In each trial a fixation cross appeared for a random duration between 1 and 2 s. Following the offset of the fixation cross, a field appeared containing three upright and three inverted faces pseudorandomly positioned on a noisy background. Faces in the search array consisted of randomized genders (three males and three female) and emotional expressions (two happy, two fearful and two neutral). Each pseudorandom stimulus was presented no more than once, none were shared across blocks, and all patients viewed the same sequence of stimuli in a given block, while block order was randomized across subjects. Subject 1 completed four blocks
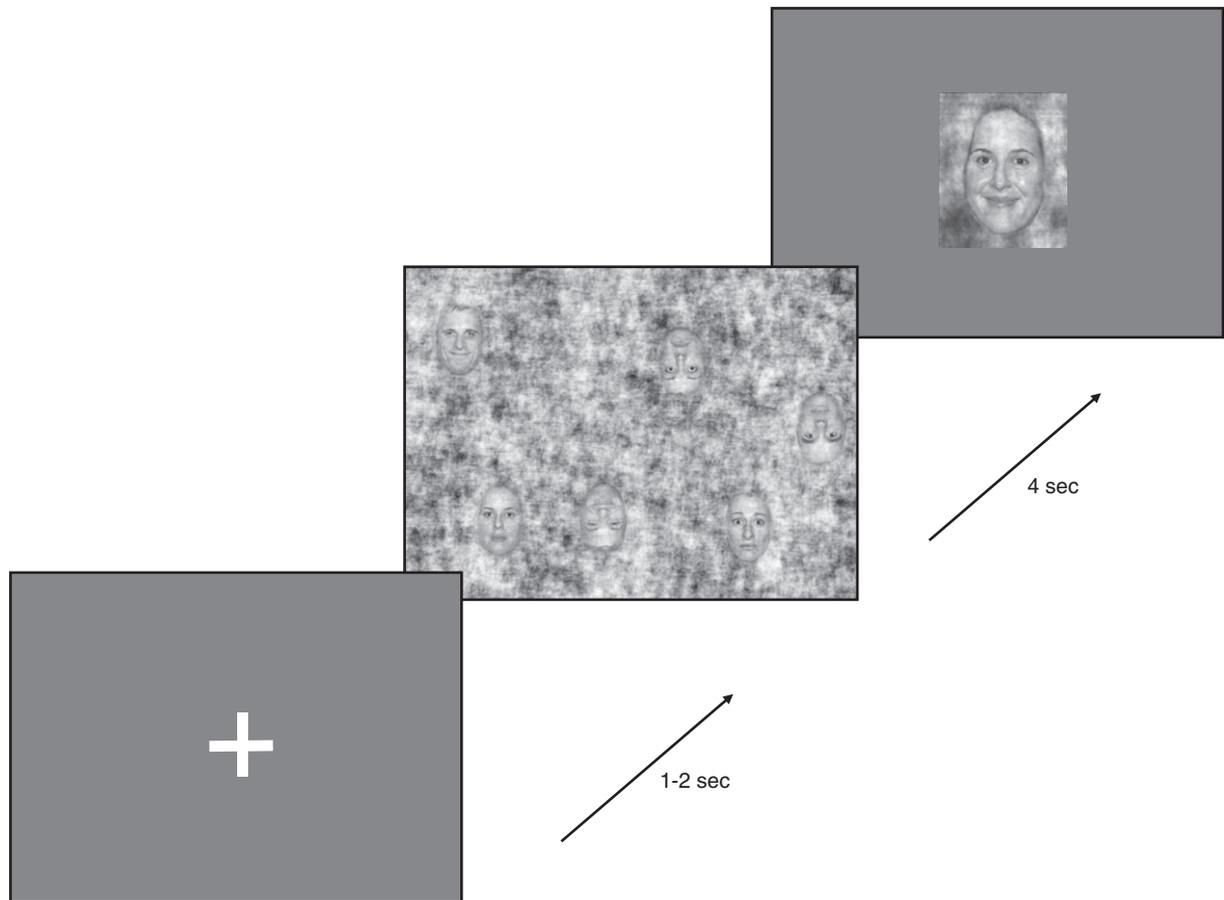
Fig. 1. Sequence of events in a trial. A fixation cross is presented for 1 to 2 s, followed by a search array of pseudorandomly positioned faces for 4 s, followed by a probe face for 1 s. Subjects indicate with a button press whether the probe face matched any face in the preceding array with respect to orientation, identity and facial expression.

and all others completed 2. Faces subtended approximately 2 deg. horizontal and 4 deg. vertical arc and were randomly positioned on a field approximately 26 by 20 deg. The minimum center-to-center distance between faces was about 4 deg. Subjects were instructed to remember either upright or inverted faces, according to block. After 4 s, the search stimulus was removed and then a probe face was presented following a randomized approximately Gaussian delay with mean 0.5 s and s.d. 0.05 s. The probe face remained visible for a random Gaussian interval of 1 s with s.d. 0.1. Using a button press, subjects indicated whether the probe face matched any of the target faces from the previous search array in both identity and facial expression.

Eyetracking

Eye movements were monitored with a remotely mounted infrared video eye tracking system (ASL 6000, Applied Science Laboratory, Bedford, Mass.), which sampled gaze position at 119.65 Hz. Effective resolution of gaze position was typically between one and two degree of visual arc.

The electrooculogram (EOG) signal was also collected in one subject (patient 3) using a 4-channel montage referenced to the mid forehead. Two electrodes were placed near the outer canthi of the left and right eyes and two above and below the right orbit. The signal was first bandpass-filtered from 1.6 Hz to 1000 Hz and then decimated to 2034.5 Hz before offline storage.

We identified saccade onsets using a velocity threshold algorithm described by Engbert and Kliegl (2002) and implemented in Matlab scripts made available by these authors for download at http://www. agnld.uni-potsdam.de/~ralf/MS/. Briefly, eye velocity was estimated over a moving average of five samples. Periods when estimated

velocity exceeded 6 standard deviations for at least 3 samples (25 ms) were identified as saccades. Saccade onset, duration, direction and amplitude were computed from extracted saccades.

Analysis of iSSP

We computed the mean amplitude and waveform of the intracranial saccadic spike potential (iSSP) in two ways. In the first analysis we computed the average time-locked to unaltered saccade onsets as extracted from the eye-movement data. We developed the second analysis in order to address the problem of systematic bias in the estimate of mean iSSP amplitude and waveform, which arises from timing error in saccade extraction. Inevitably, some error is introduced from noise in the gaze position signal and by the sampling period of the eye tracker, which at 8.3 ms falls below the Nyquist frequency for most of the spectral range of the iSSP. Both factors are expected to contribute to significant variability in the alignment of phase of the iSSP across fixations. As a consequence of such timing error, average iSSP amplitude would be underestimated, and the contribution of high frequencies attenuated, especially above the Nyquist frequency of the gaze position sampling. We therefore improve the timing of saccade onset extraction on the basis of the oEMG contamination, itself, which has greater temporal precision than the gaze record, and adequate signal to noise ratio in selected channels to be detected in the raw data (e.g. Fig. 2A). This "corrected" saccade onset time was computed from peaks in the 20–200 Hz power within the channel with the greatest average saccade-onset associated band-power increase. Selected channels are listed in Table 1. In the first step the data were bandpass filtered between 20 and 200 Hz, and the complex analytic signal was obtained from the Hilbert transform. The complex modulus of the Hilbert transformed signal gives

the instantaneous amplitude envelope. For each subject the channel with the largest mean perisaccadic increase in log envelope was selected for further processing, and the corrected onset times extracted from this channel were used in the alignment of all others. Within a 200 ms window centered on each saccade onset extracted from eye-tracking data, the 20–200 Hz band envelope from the selected channel was weighted by a Hanning window and the maximum of the weighted signal within the window became the point of alignment in subsequent averaging. The resulting shift in the onset time fell within a narrow peak (95% interval of approximately 50 ms width) offset by between −40 to +10 ms across subjects with respect to the originally extracted saccade onset time (Supplemental Fig. 1). Note that this procedure does not introduce systematic bias in the estimate of iSSP peak-to-trough amplitude because the correction was made with respect to the signal envelope, whereas iSSP amplitude was estimated from the average of the raw signal. The envelope-shifted average therefore reflects the systematic relationship between phase and power envelope. For a signal with a random phase-envelope relationship, the procedure is expected to increase the variance of the estimate but not to result in a systematic positive or negative bias. This procedure was only applied in estimating the mean iSSP waveform and peak-to-trough amplitude, and not to estimates of peri-saccadic spectral and band-power perturbation described in following sections, as the procedure is expected to introduce systematic bias in the average of signal power.

In computing both corrected and uncorrected averages, only saccades which fell within the 4-s duration of a trial were included in the analysis, and all available blocks were included for each subject. The number of included trials was 288 for subject 1 and 144 for all others, and the number of saccades onsets was 3318, 1402, 1372, 1571, and 1327, respectively. Peak-to-trough amplitude averages were computed as the average voltage difference between fixed peak times, with respect to corrected saccade onsets. For each subject, peak

Table 1
Maximal iSSP peak-to-trough amplitude and location for each subject. X-, Y-, and Z-values give the MNI-space coordinates for the contact with the largest iSSP in each of the 5 subjects.

Subject	Structural label	X	Y	Z	iSSP Amp (µV)	SEM
1	Parahippocampal gyrus	−21	2	−30	44.1	0.6
2	Temporal pole	−21	13	−37	56.4	1.1
3	Temporal pole	24	11	−41	22.6	1.0
4	Temporal pole	30	15	−38	54.2	1.2
5	Temporal pole	−26	16	−38	43.0	1.1

times were extracted from the channel with maximal saccade onset band power perturbation. Peak times were not observed to vary substantially between channels (although in a few cases polarity reversed), and peak-to-trough amplitude was computed for all channels at the same extracted peak times. Statistical analyses of amplitude were carried out by applying a two-tailed t-test (H_0: $\mu = 0$). To correct for multiple comparisons, we applied false discovery rate (FDR) criteria to P-values across all channels (Benjamini and Hochberg, 1995; Benjamini and Yekutieli, 2001). We considered a channel to have a significant iSSP response if the P-value corresponded to a false discovery rate q value, less than or equal to 0.01, where q is the expected proportion of falsely rejected null hypotheses across all significant tests.

Comparison of the envelope-shifted iSSP (averaged with respect to corrected saccade onsets) and the unshifted iSSP (using uncorrected saccade onsets) revealed that the unshifted iSSP had a comparatively smaller peak-to-trough amplitude (median ratio 0.52 for all channels in which iSSP exceeded 10 µV) and attenuation at higher frequency, both of which are expected from random timing error. We also observed decreased variance of peak-to-trough amplitudes after shifting (median decrease of standard deviation, 4.83, 4.62, 0.41,
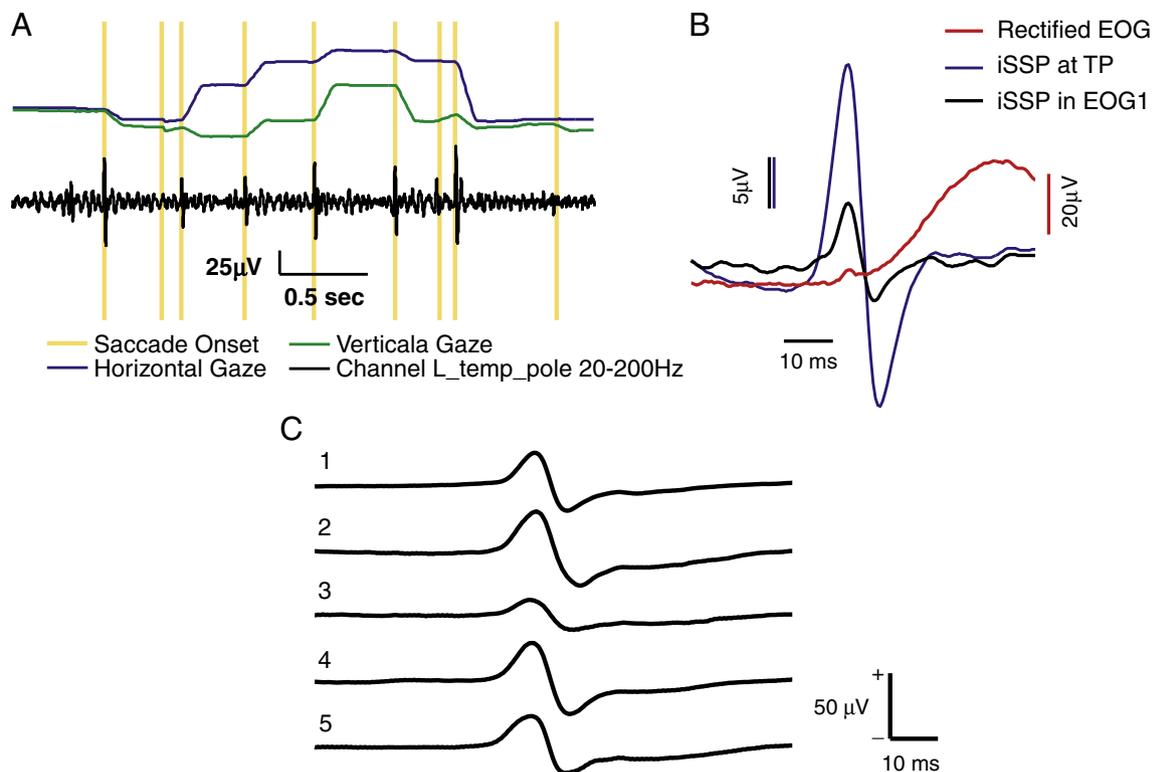

Fig. 2. The intracranial Saccadic Spike Potential. (A) Saccadic spikes observed in unaveraged 20–200 Hz filtered field potential (black line) from a contact near temporal pole. The top two plots show horizontal and vertical gaze position. Yellow lines indicate extracted saccade onset times. Note that the second saccade onset most likely represents a false positive. (B) Morphology of the iSSP averaged with respect to saccade onset in an intracranial channel (blue line) and as observed in extracranial EOG contact (black line). In both cases data are bandpass filtered from 20 to 200 Hz. Average rectified unfiltered EOG (red) shows the time course of the iSSP in relation to onset of eye movement. (C) iSSP morphology in all five subjects observed in the channel with maximal peak-to-trough iSSP amplitude. In all subjects the maximal iSSP amplitude appeared in channels near the temporal pole.

4.75, 3.38 μV for each subject, respectively, across all channels in which iSSP amplitude exceeded 10 μV), consistent with a reduction of inter-trial alignment error. We note that this procedure is useful for obtaining a more temporally precise estimate of eye movement onset based on the combination of eye-tracking and oEMG signal because the saccadic spike bears a close and consistent relationship with the onset of eye movement (Keren et al., 2010). All data on the iSSP peak-to-trough amplitude, as well as mean waveform use the corrected saccade-onset times, whereas all data on perisaccadic band-power and spectral perturbation use the uncorrected saccade-onset times.

To evaluate the dependence of iSSP amplitude on saccade amplitude and direction, we examined the iSSP in the EEG channel with the largest amplitude iSSP in each subject, normalized by the mean iSSP amplitude for saccades greater than 10 degrees, and pooled across subjects. In the pooled data, we fit an eighth-order polynomial to estimate mean peak-to-trough amplitudes as a function of saccade amplitude (Fig. 5). Separate polynomial fits were also obtained for ipsi- and contraversive saccades. In each case all saccades were considered ipsiversive if the x-component of the difference of gaze position before and after the saccade was negative (positive) for left-sided (right-sided) contacts, and contraversive otherwise. Polynomial order of 8 was chosen as it minimized bias corrected Akaike's information criterion (AICc) (Akaike, 1974; Hurvich et al., 1998).

Independent component analysis (ICA) estimation and filtering

ICA refers to a family of algorithms that find a linear projection of a multivariate signal which maximizes statistical independence of the elements of the signal under the transformation (Hyvärinen and Oja, 2000). The goal in applying ICA is to find a linear projection which "unmixes" distinct physically meaningful sources that contribute to the original signal. The algorithm assumes that sources are mutually independent and that the number of sources does not exceed the number of channels. Among other applications, it has shown promise in the isolation and removal of motor artifacts (Jung et al., 2000a; McMenamin et al., 2010) from EEG, notably the saccadic spike potential (Keren et al., 2010). In order to improve the validity of the constraint on the number of assumed source, we applied a 20 to 200 Hz bandpass filter to the signal, removing the contribution from signals outside the peak frequency range of the iSSP. This bandwith was chosen on the basis of the characteristic spectral range in which the contribution of the SSP tends to be large relative to background EEG (Keren et al., 2010; Yuval-Greenberg et al., 2008), which we find to hold for the iSSP as well (Fig. 13) We applied the Bell–Sejnowski ICA algorithm (Bell and Sejnowski, 1995), implemented in the EEGLab toolbox for Matlab (Delorme and Makeig, 2004) to each subject's data concatenated across all trials (i.e. intertrial periods were excluded).

A critical step in the application of ICA is the identification and interpretation of the resulting components. Identifying components which correspond to motor contamination may rely on properties of the signal and on the spatial distribution of the signal over receiving contacts, revealed by the coefficients of the mixing matrix (Jung et al., 2000b; Keren et al., 2010; McMenamin et al., 2010). In the present case we selected components based on the increase in 70–100 Hz power within the 100 ms window centered on saccade onset relative to the −150 to −50 ms window preceding onset and secondarily on the distribution of mixing weights. Components were identified as containing significant oEMG based on the magnitude of the response.

To filter the data of the independent components containing the greatest saccade onset-associated power increase, we removed the first 2 sorted independent components. We selected 2 as the cutoffs, as removing higher components resulted in a little additional reduction of perisaccadic power (Fig. 8) and because the dependence of iSSP amplitude on saccade direction, described in the results, implies at least two sources, corresponding to left and right extraocular muscle

groups. Filtering was done by nulling the corresponding rows of the mixing matrix and projecting back into the space of the original signal, which gives a linear transformation of the original data:

$$X^* = QX$$

where Q is the product of the modified mixing matrix, M^*, in which the columns corresponding to the discarded independent components are set to zero, and the unmixing matrix: $Q = M^* M^{-1}$.

Wavelet analysis

Time-frequency spectral estimates were computed using the complex Morlet (Delprat et al., 1992) wavelet. The time-varying spectral estimate S at time t and frequency f is given by the convolution

$$S_\alpha(t,f) = \int X(s) W_\alpha(t-s,f) dt$$

where

$$W_\alpha(t,f) = \left(\left(\frac{\alpha}{2\pi f} \right)^2 \pi \right)^{-\frac{1}{4}} \exp\left(-2t^2 \left(\frac{\pi f}{\alpha} \right) + 2\pi i f t \right)$$

Power at each time and frequency point is given by the squared modulus of the complex value, S. The bandwidth parameter, α, was chosen to be 7. Data were normalized at each frequency bin by subtracting the average log power in a preceding reference period. In each case the average of the log power was used rather than the log of the average power in order to reduce the effect of the large positive skew in the distribution of power. Results, however, were not found to depend heavily on the choice of transformation. Data were rescaled into dB by multiplying with a factor of $10/\log(10)$.

We obtained time-frequency plots of log spectral power averaged around the time of saccade onset by first computing the wavelet transform for the entire duration of the recording across 4 Hz–200 Hz, and then computing the average of log power within a 1000 ms window centered around the saccade onset. Average power was normalized in each frequency band by subtracting average log power in the −500 to −200 ms window preceding the saccade onset. Time frequency plots averaged with respect to onsets of the search array ("trial-onset average") were obtained similarly and normalized by the −400 to −100 ms baseline fixation period preceding the trial onset. Only saccades whose onsets fell within the 4-s duration of the search stimulus were included in the analysis. For statistical analysis we applied a paired t-test on the difference between log power in the stimulus period and mean spectral power in the baseline fixation period at each time point. Statistical tests accounted for multiple comparisons by applying the false discovery rate adjustment (FDR) (Benjamini and Hochberg, 1995) across all time-frequency points and all channels.

Perisaccadic power

In order to evaluate the effect of saccade onset-related spectral perturbation around the observed spectral peak for the iSSP, the signal was filtered from 70 Hz to 100 Hz with a high order FIR bandpass filter, and mean power was computed within a sliding 50 ms window. The 70–100 Hz band was chosen because it lay near the middle of the observed iSSP related broad-band spectral response, and because it avoids possible line noise at multiples of 60 Hz. Average log power was computed time-locked to saccade onset, detected by the eye tracker (without using envelope alignment, see above) and to trial onset. We evaluated perisaccadic band power perturbation by normalizing to mean power in a −150 to −50 presaccadic baseline period which tended to fall within the duration of the preceding fixation (green bar in

a top left panel of Fig. 13). Trial-onset averages were normalized with respect mean power in the preceding −400 to −100 ms window. For statistical analysis we applied paired *t*-tests on the difference between log power in the test period and the baseline fixation period. Statistical criteria were adjusted for multiple comparisons by applying false discovery rate (FDR) criteria across all time points and channels. We considered a channel to show significant evidence for spectral perturbation if the minimum *P*-value corresponded to a FDR *q*-value of 0.01 or less.

Contribution of the iSSP to spectral and band-power perturbation

Because changes in perisaccadic power may reflect cortical sources as well as iSSP, we evaluated the contribution of iSSP by observing the effect of ICA filtering on the band-pass power between 70 and 100 Hz and in wavelet spectrograms ranging from 4 to 200 Hz. In both cases the same wavelet and power spectral analyses described previously were carried out before and after ICA filtering (Figs. 10, 12, 13). Four separate contrasts on log power were computed: (1) the increase over baseline before filtering, (2) the increase over baseline after filtering, (3) the differences in the increases over respective baselines between filtered and unfiltered data, and (4) on the difference of log power between filtered and unfiltered data within the respective epochs without normalization to the respective baseline. In each case statistical validation was carried out as paired *t*-tests, with significance criteria set by false discovery rate (FDR $q = 0.01$).

Contrasts 1 and 2 are shown in Figs. 10, 12, 13. Contrast 3 is performed on the difference spectrograms shown in Figs. 12 and 13, while contrast 4 is shown for band power within the 0–500 ms post trial onset epoch in Fig. 10D. Contrast 4 gives an estimate of the contribution of the two filtered independent components to overall power. Contrast 3 is less sensitive to the presence of the signal than 4 because it does not remove residual variability within each epoch. It gives a better measure of the practical consequence of contamination, however, as it reflects the change in power arising from the correlation between saccade frequency and stimulus onset.

Multitaper coherence

We computed interchannel coherence using Thomson's multitaper spectral estimators (Thomson, 1982) within two 100-ms windows centered at −100 ms and 0 ms relative to unshifted saccade onset. Multitaper spectral estimates were obtained by multiplying the data in the window of observation with two orthogonal tapers from the discrete prolate spheroidal sequence (DPSS), which optimally suppresses spectral leakage outside the window of resolution, resulting in effective frequency resolution of 15 Hz. Total spectral power and cross-spectral power were computed as a weighted sum across the two tapered windows.

Coherence was computed pairwise for all channels using the formula

$$C_{ij}(f) = \frac{\sum\limits_{t,w} \lambda_t S_{wti}(f) S_{wtj}^*(f)}{\sqrt{\left(\sum\limits_{t,w} \lambda_t |S_{wti}(f)|^2\right)\left(\sum\limits_{t,w} \lambda_t |S_{wtj}(f)|^2\right)}}$$

where $S_{wti}(f)$ is the multitaper spectral estimate for the *w*th window, *t*th taper and *i*th channel. The factor λ_t is the eigenvalue associated with the *t*th taper, and is close to 1 for the DPSS tapers used. The parameter w sums over all saccades included in the analysis.

A bootstrapped distribution for the difference of coherence between the presaccadic window and the saccade-onset window was obtained by recomputing coherence from the original data after randomly resampling with replacement. 250 bootstrapped estimates were computed and statistical thresholds estimated from the resulting empirical distribution. For the purpose of display in Fig. 15, a change in coherence was considered significant if zero fell outside the $P > 0.008$ two-tailed confidence interval (that is, if the smallest bootstrap estimate among the 250 exceeded zero or the greatest estimate was less than zero) at more than half of the frequency samples in the 40–100 Hz range. Only values that meet this criterion are plotted.

Image coregistration

Because the iSSPs are similar across subjects in terms of amplitude, morphology (Fig 2C), and distribution, analyses of iSSP distribution were carried out on average waveforms pooled across subjects. For each subject, electrode locations for subtemporal and depth electrodes were manually identified in a CT volume coregistered to a T1 structural MR scan. All individual T1 images were coregistered with the MNI152 whole head template image (Evans et al., 1993) using a seven-parameter linear transformation which permitted rotation, translation and global rescaling. The parameters were estimated using an unsupervised nonlinear optimization method implemented in the FSL toolbox (Jenkinson and Smith, 2001; Smith et al., 2004), with normalized correlation as the cost function. We used the seven-parameter linear transformation in order to preserve spatial isotropy.

Cortical surface renderings were generated from the T1 image of patient 4. In order to project contact locations on the rendered image, locations for all subjects were transformed from the reference space into the image space for patient 4 using the inverse of 4's transformation obtained in the previous step. The co-registered locations were visually inspected in both the reference volume and the surface rendering to verify accurate correspondence between the original location and the transformed location.

Because CT imaging artifact made the identification of individual contact locations difficult in the densely spaced lateral grids, we applied a different procedure in the coregistration of lateral grid contacts. Contact locations for the lateral grids were determined from intraoperative digital photographs on the basis of sulcal and gyral landmarks. These were projected onto 2D renderings of the lateral view of the cortex. For each subject the lateral 2D rendering was registered to that of patient 4 using a linear transformation which minimized squared distance between a set of manually selected fiducial points.

For all contacts in which iSSP exceeded 10 μV (which did not include any of the lateral grid contacts), MNI coordinates are reported in Supplemental Table 1. Reported structural labels are obtained through FSL from the Harvard-Oxford probabilistic atlas (Caviness et al., 1996). In each case the reported structure has maximum probability at the reported MNI coordinate.

Non-specific artifact identification

We identified trials which contained possible artifacts, nonspecific to eye movement, using a threshold criterion on the raw signal. Samples which deviated more than 5 s.d. from the mean were flagged as outliers. Rejecting trials within each channel which contained any outliers of 5 s.d. or more over the course of the trial resulted in a median rejection rate across channels of 2.4% , 4.2%, 9.7% , 5.2%, 4.2% trials respectively for subjects 1 to 5, with 2.5% to 97.5% inter-quantile intervals of (0.3%, 10.1%) , (0%, 24.3%) , (2.1%, 22.3%), (0 %,24.3%), (0% ,13.2%), respectively. In most cases outliers were caused by interictal discharges, and channels in which rejection rate was high showed frequent interictal activity. Because interictal discharges did not interfere with the observation of the iSSP, and because discarding trials did not appreciably change the results, we included all trials and channels in the presented analysis.

Results

The intracranial saccadic spike (iSSP)

In all five patients, the onsets of saccades were associated with a biphasic potential, the intracranial saccadic spike (iSSP) (Fig. 2),

which closely resembled the scalp saccadic spike in waveform and time course (Becker et al., 1972). The response was observed both in subdural ECoG (Fig. 3) recordings and in depth recordings from anterior temporal lobe and Heschl's gyrus (Fig. 4). Peak-to-trough amplitude differed significantly from zero at a majority of contacts in most subjects over all observed regions. The numbers of contacts in which amplitude reached significance were 124, 88, 52, 120 and 123 respectively for subjects 1 to 5, out of 128 channels in each subject. Amplitude was greatest near the temporal pole and remained substantial mesially and anterior to the brainstem, with a magnitude greater than 10 μV over roughly the anterior half of the ventral temporal surface. Locations and amplitudes for the channels with the largest iSSP in each subject are listed in Table 1, and all channels with amplitude greater than 10 μV are listed in Supplemental Table S1. The response also showed a large medial to lateral gradient, diminishing at more lateral contacts and in a few cases reversing polarity at anterior ventrolateral contacts. This pattern is particularly apparent in depth electrodes and in ventral ECoG grids. In depth contacts targeted to anterior medial temporal lobe, iSSP amplitude decays sharply with increasing laterality (Fig. 4). In all subjects, the reference electrode

was located outside the skull, embedded below the galeal membrane near the vertex. Thus, the possible contribution of the reference electrode to contamination is an important issue, which we will consider in further detail.

Effect of saccade amplitude

The visual search task encourages subjects to generate frequent large amplitude saccades, which may tend to exaggerate the severity of any eye movement related contamination. We therefore examined the dependence of oEMG contamination on saccade amplitude. The distribution of saccade amplitudes was bimodal (Fig. 5), reflecting a subset of saccades which remained within faces and another which switched between faces. The former fell below 4 degrees amplitude and the latter were typically greater than 4 degrees, reflecting the minimum distance between faces. Because subjects generated a wide range of saccade amplitudes over the course of the task, the data allow an examination of the dependence between saccade amplitude and oEMG contamination. We observed that iSSP amplitude depended on saccade amplitude in a nonlinear fashion, with a rapid increase for
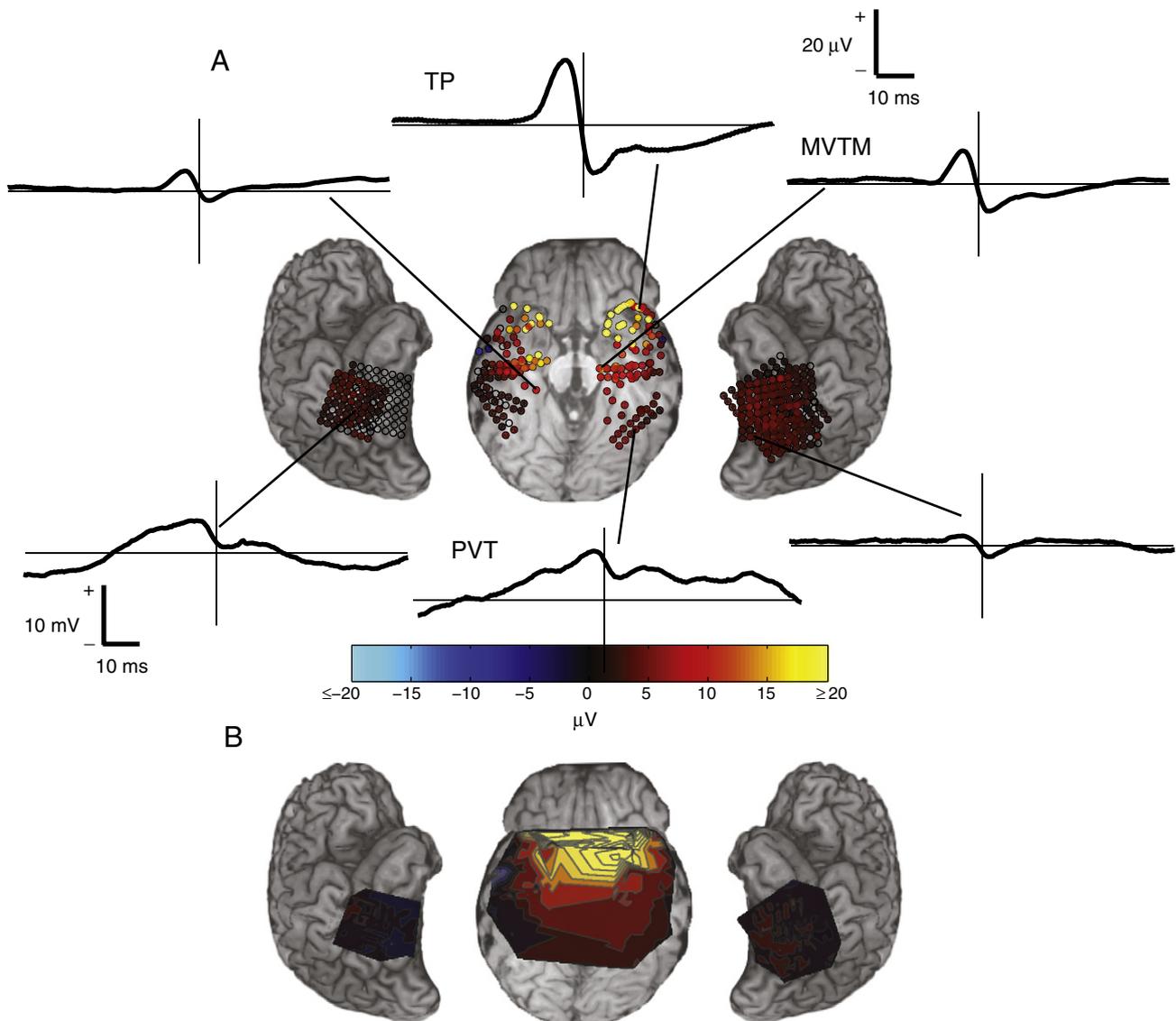

Fig. 3. Manifestation of iSSP in subdural ECoG recordings. (A) At center, peak-to-trough amplitudes of the iSSP recorded in channels which reached statistical significance at FDR *q*-value = 0.01. Channels which did not reach the significance criterion are unfilled. Six example waveforms are displayed for the indicated contacts. Note that the vertical scale for the waveforms from posterior contacts differs from anterior contacts in order to aid visibility. (B) Peak-to-trough amplitude interpolated over all contacts and subjects.
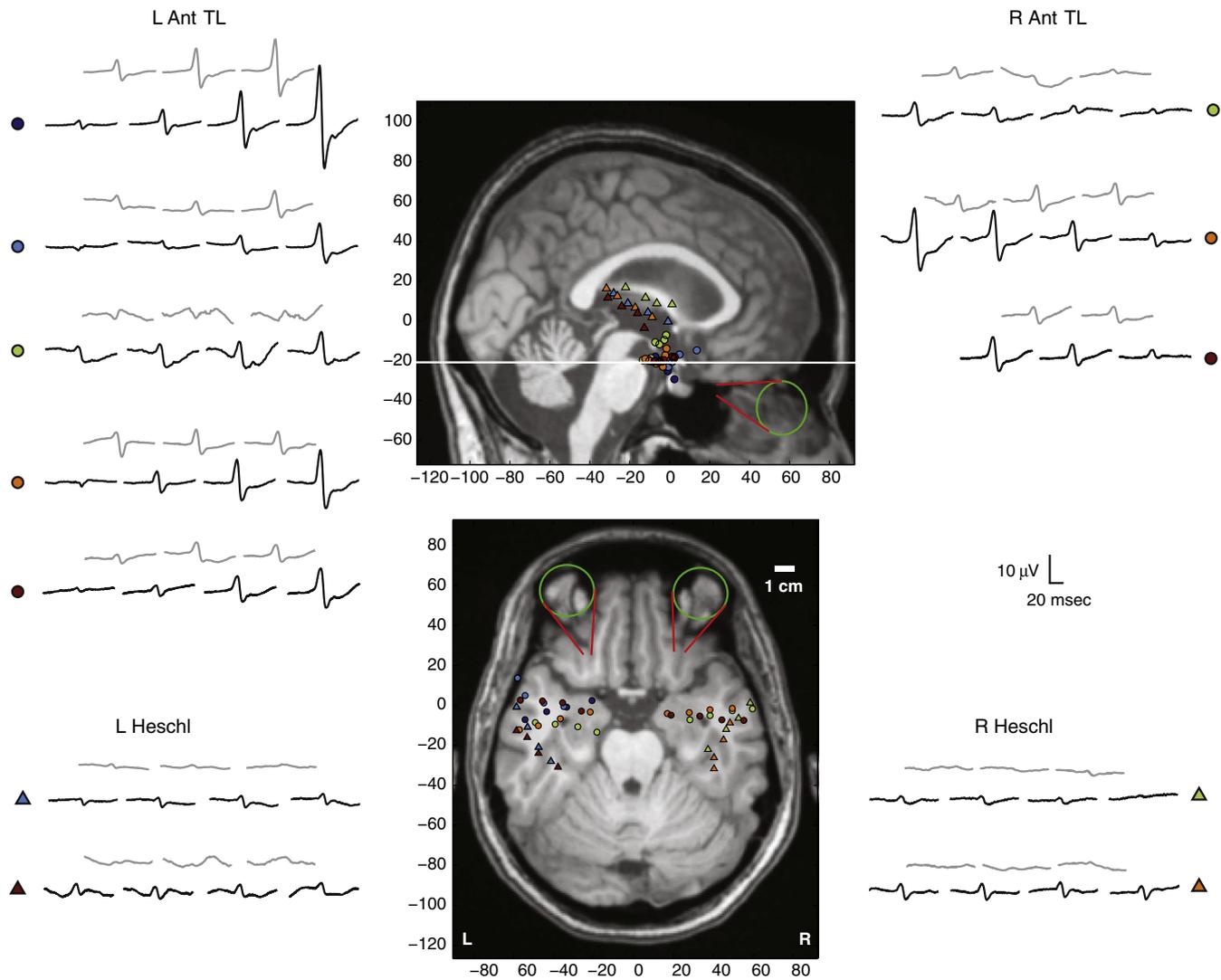
Fig. 4. Manifestation of iSSP in depth recordings from anterior temporal lobe and Heschl's gyrus. In four contact depth electrodes targeted to left (all subjects) and right (subjects 3, 4 and 5) amygdala (circles), large amplitude iSSPs are observed at medial contacts. Smaller iSSPs appear at contacts in Heschl's gyrus (triangles). Left and right columns show mean iSSP for each contact arranged in left-to-right order under common subgaleal reference (black) and after bipolar rereferencing between neighboring channels (gray). Contact location is shown in the central column, where color indicates subject identity. As in the subdural ECoG electrodes, a large medio-lateral gradient is apparent in iSSP amplitude. Eye and extraocular muscle (medial, lateral, superior and inferior rectus) position are shown schematically with green ellipses and red lines, respectively. The most medial right-sided contact for subject 5 was broken and is not shown.

saccades of less than 8 degrees, approaching a stable plateau beyond 8 degrees (Fig. 5). For saccades of 2 degrees, the mean iSSP amplitude averaged across all subjects was 33% of the value at the plateau, taken as the mean for saccades above 10 deg, and 43% of the mean across all saccades. The significance of the nonlinearity was confirmed by a sequential likelihood ratio test on the polynomial terms, for which each additional term reached a significance threshold of $P<0.01$ up to the fourth order term. The data were fitted with an 8th order polynomial, as this order minimized Akaike's information criterion (AIC). The iSSP amplitude also showed significant dependence on saccade direction: at the temporal pole, ipsiversive saccades were associated with larger iSSPs than contraversive (Fig. 5). These observations agree with the amplitude and direction dependence reported for the scalp SSP (Boylan and Doig, 1989; Riemslag et al., 1988; Thickbroom and Mastaglia, 1986).

The nonlinearity of the response suggests that the practice of discarding intervals which contain saccades above some amplitude threshold may not reliably eliminate contamination. In particular, thresholds based on the EOG signal may be insensitive to small

amplitude saccades, as eye-movement related deflections in EOG scale linearly with saccade amplitude (Yuval-Greenberg et al., 2008). We therefore examined the dependence of mean iSSP amplitude across all channels for saccades which fell in amplitude intervals of 0° to 2° (median $N=270$), 2° to 4° (med. $N=163$), 4° to 6° (med. $N=194$), 6° to 8° (med. $N=220$), and 8° to 10° (med. $N=225$). For all subjects iSSP amplitude and the proportion of channels in which significant peak-to-trough amplitude was observed increased with saccade amplitude up to 6° to 8° and leveled off in the 8° to 10° range, agreeing with the aforementioned nonlinearity (Figs. 6 and 7). In all subjects a large fraction of channels showed significant iSSPs at all saccade amplitude intervals greater than 4 deg. A significant response also remained in a subset of channels for saccades of less than 2° (median 8 of 128, range 2 to 20) over the anterior third of the ventral temporal surface. For saccades of 2°–4° the median number of significant channels was 28 with a range of 15 to 41. For the remaining amplitude intervals the medians were 42, 46 and 51. Small amplitude saccades of less than 2° therefore generated a detectable iSSP with a more restricted distribution than larger amplitude saccades.
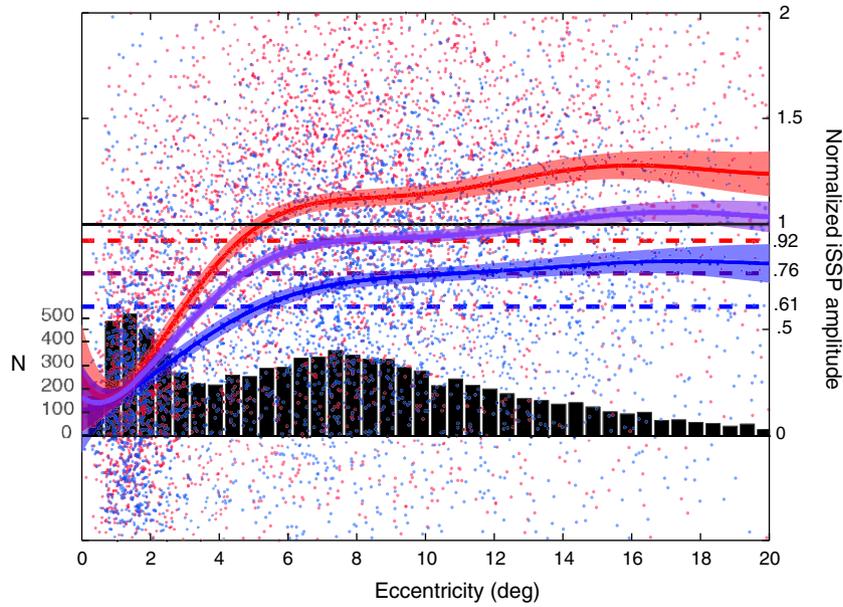
Fig. 5. iSSP peak-to-trough amplitude dependence on saccade amplitude and direction. Peak-to-trough amplitudes in unaveraged data, normalized within each subject to the mean iSSP amplitude for all saccades over 10 deg. Data are taken from the channel with the largest iSSP, which was a contact near temporal pole in each subject, normalized and pooled across subjects. Mean iSSP amplitude as a function of saccade amplitude and 2 SEM are shown for ipsiversive saccades (red), contraversive saccades (blue) and all saccades (purple) in data pooled across subjects. Curves are fitted by an eighth order polynomial, with the order chosen to minimize AIC. iSSP amplitude increases approximately linearly for small amplitude saccades under 5 deg, approaching a plateau beyond 6 degrees. In all subjects ipsiversive saccades generated a larger iSSP than contraversive at the selected temporal pole contact. Mean iSSP amplitude over all saccades in each case is shown by the dashed lines of corresponding color. The histogram shows the relative frequency of saccades as a function of eccentricity.
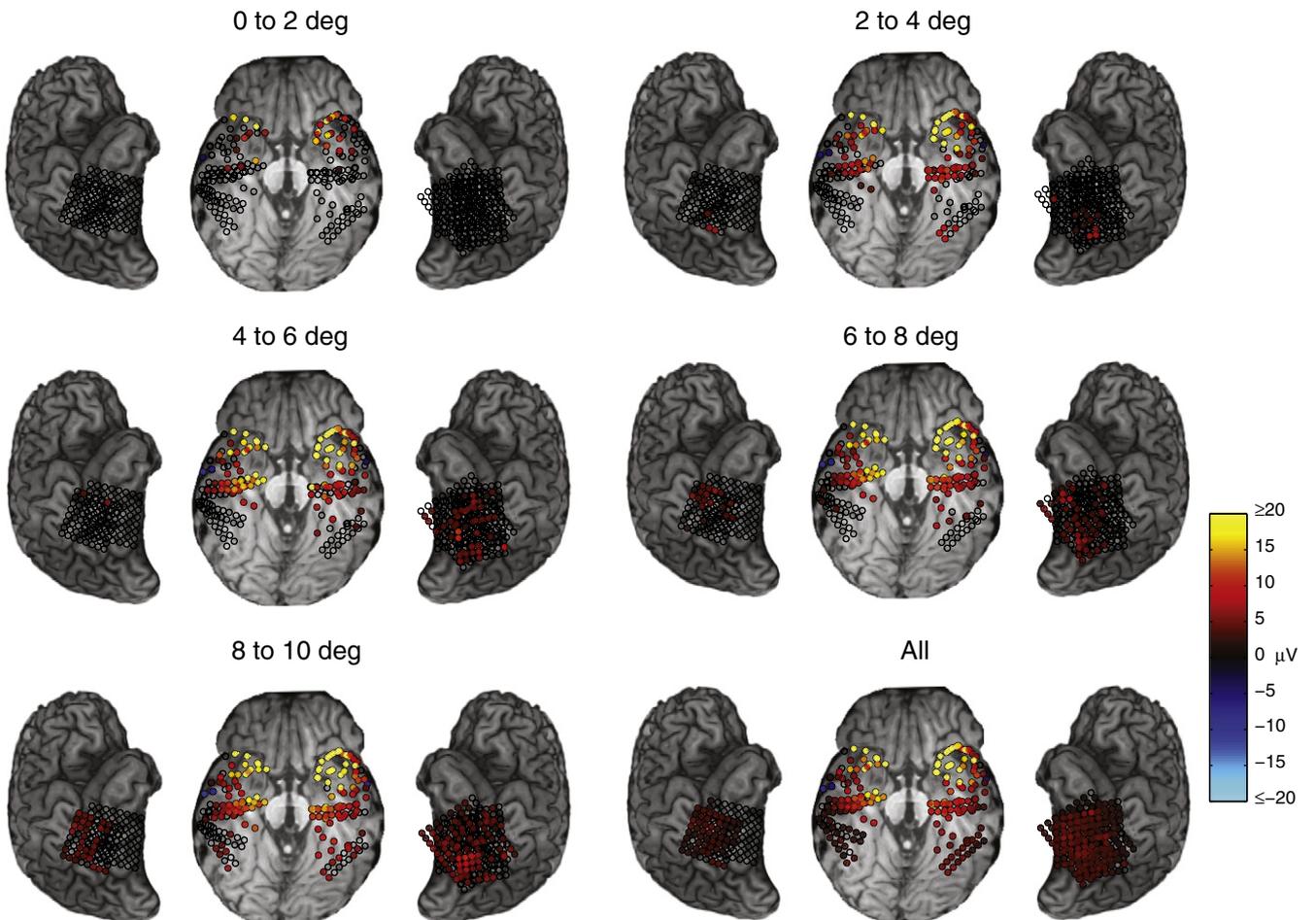

Fig. 6. Dependence of the distribution and peak-to-trough amplitude of saccadic spikes on saccade amplitude. The color scale shows mean iSSP peak-to-trough amplitude for saccades which fall within the given amplitude range. Only channels which reached an FDR corrected significance threshold $q \leq 0.01$ are filled.

ICA filtering

In order to better characterize the contribution of the oEMG signal to the observed responses and to explore methods for removing the contaminant, we applied independent component spatial filtering (ICA) to the signal. ICA has shown promise in reducing contamination from oEMG and other myogenic sources (Keren et al., 2010; McMenamin et al., 2010) in scalp EEG recordings. In all subjects sorting of independent components returned a single component with a large iSSP waveform and one or two other components in which residual oEMG was discernible in the band-pass filtered mean perisaccadic power (Fig. 8). In each case the distribution of mixing weights of the first sorted component closely resembled the distribution of iSSP peak-to-trough amplitudes, and spikes were readily observed in the band-pass filtered unaveraged data. To suppress oEMG contamination we removed the first two sorted components, as removing further components provided little apparent improvement, and because at least two source are required to

explain the dependence between horizontal saccade direction and iSSP amplitude. To evaluate the effectiveness of this procedure we compared iSSP amplitude (Fig. 9) and perisaccadic wavelet power (Fig. 13) before and after filtering, as well as the effect of filtering on spectral perturbation time-locked to trial onset (Figs. 10 and 12), and interchannel coherence (Fig. 15). Residual iSSP amplitude and change in perisaccadic power at contacts near the temporal pole, visible in Figs. 6 and 7, most likely reflects residual oEMG contamination affecting mainly channels nearest the oculomotor sources.

Bipolar rereferencing

We examined the effectiveness of bipolar rereferencing (BPR) in suppressing contamination. BPR is a simple form of spatial filtering that applies a difference between selected pairs of neighboring channels. Like ICA filtering, BPR reduced the extent of the iSSP beyond the temporal pole, as measured by iSSP amplitude (Fig. 9) and coherence (Fig. 15). The amplitude of the iSSP was diminished, but it
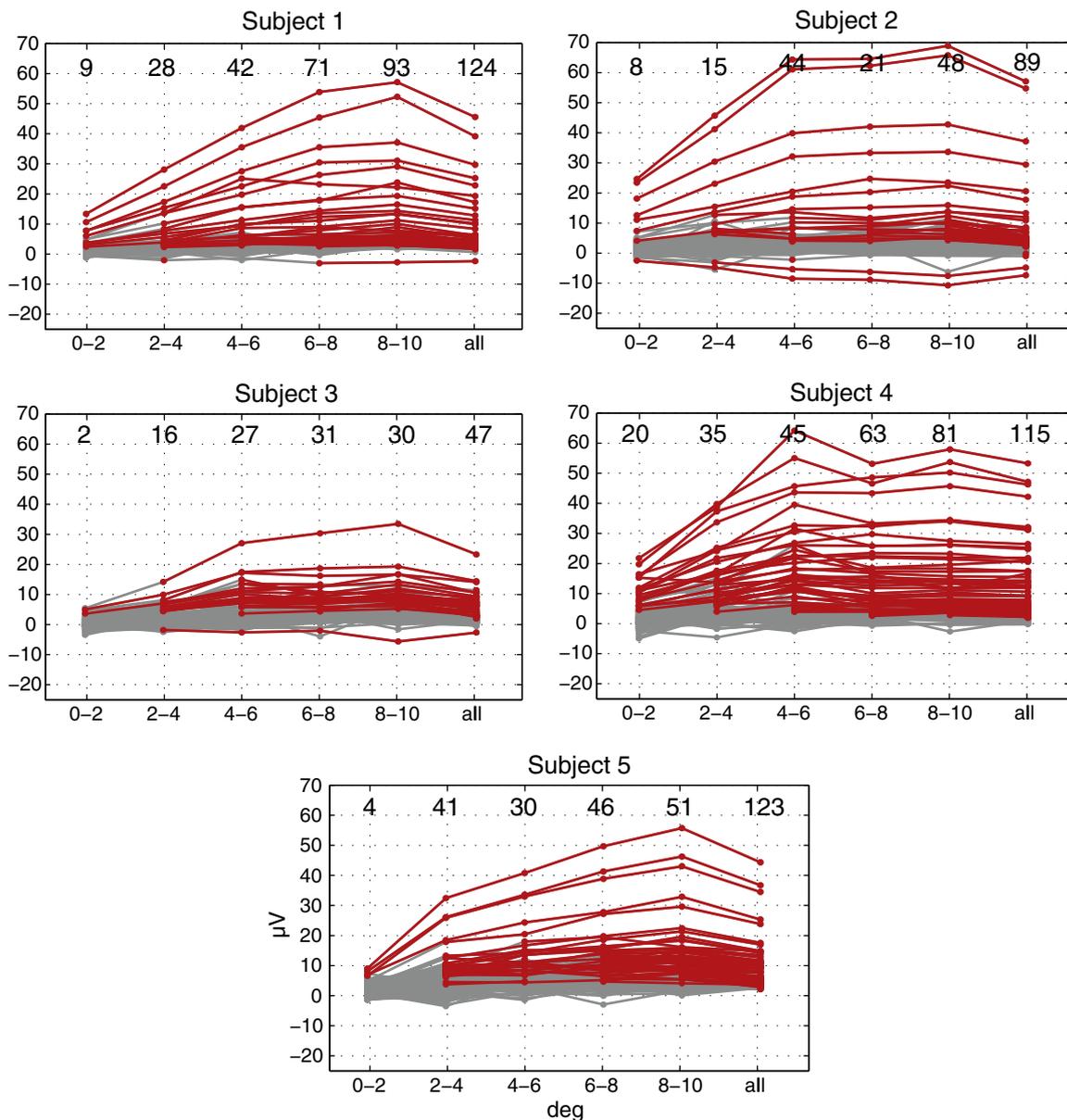

Fig. 7. Dependence of peak-to-trough iSSP amplitude on saccade amplitude across channels. Mean peak-to-trough amplitude is shown for saccades which fall within the given amplitude range. Responses are colored red if they are significantly different from 0 at FDR corrected significance threshold $q \leq 0.01$. Values at the top of each panel show the number of channels, out of 128, meeting the significance criterion within each interval.
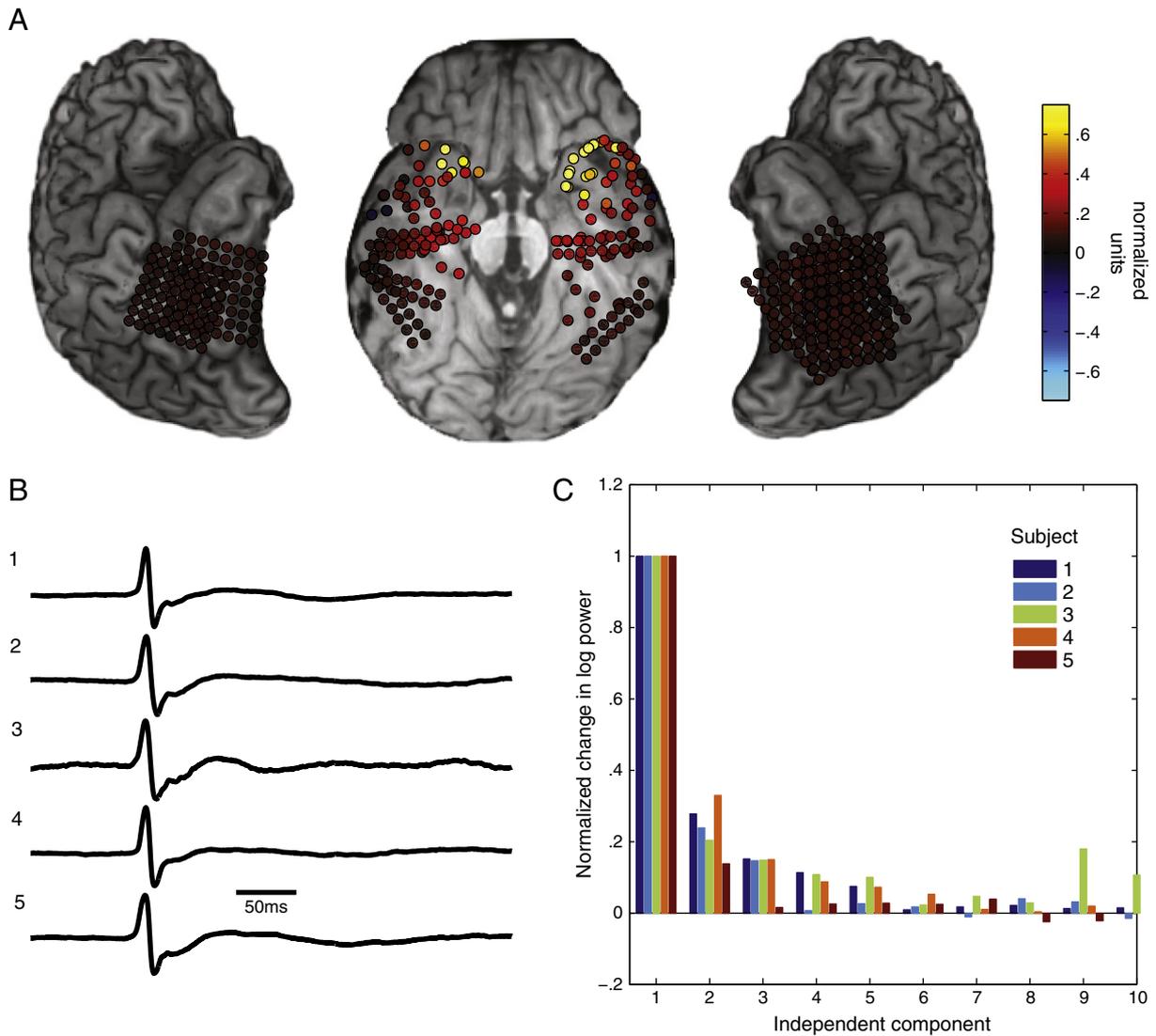
Fig. 8. Independent Component Analysis to remove the iSSP related signal. (A) Distribution of mixing weights for the component with the largest iSSP related gamma band spectral perturbation of band power. (B) iSSP waveform in the independent component with the largest perisaccadic perturbation (shown for each of the five patients). For both A and B the units of components and weights returned by ICA are arbitrary and have therefore been normalized within each subject to the maximum weight across all channels in the former case and to the peak-to-trough difference in the latter. (C) Decrease in perisaccadic 20–200 Hz log spectral perturbation for the channel with the largest iSSP after removing the kth sorted IC component (sorted by perisaccadic perturbation), normalized for each subject (different colors) to log change after removing the first component.

remained significant in many of the channels near the anterior half of ventral temporal cortex. Combined ICA and bipolar rereferencing resulted in the most effective suppression of iSSP amplitude, however in all cases residual contamination remained near the temporal poles.

Saccade-related band power and spectral perturbation

In channels near the temporal poles and in all patients, wavelet time-frequency analysis revealed a broad increase in power above 20 Hz, within the 100 ms window around saccade onset (Fig. 13). This response is attenuated further from the pole and absent at posterior contacts. Representative examples of wavelet spectrograms are shown at the respective locations: contact TP near temporal pole, MVTM near the mesial section of middle ventral temporal cortex, and PVT over posterior ventral temporal cortex. In the period −150 to −50 ms before saccade onset, which typically fell within a period of stable fixation (Fig. 13), contacts TP and MVTM showed a decrease of power in the same frequency band with respect to the baseline period (left upper and middle panels in Fig. 13). In both the trial onset average (Fig. 12) and the saccade onset average (Fig. 13), responses in TP and to a lesser extent

MVTM closely tracked the histogram of saccade onsets, a consequence of the saccade onset associated spectral perturbation. Across trials, the first saccade following the stimulus onset fell within a characteristic interval of between 200 and 300 ms, leading to a peak in both the histogram of saccade onset times and the wavelet spectrogram at contact TP and to a lesser extent at MVTM. A second smaller peak appears between 400 and 600 ms after the termination of the first fixation. The initial peaks are followed by a prolonged elevation in gamma power over the remaining duration of the trial.

Although saccade onset-related changes are easy to show in the saccade-triggered averages, a key question is whether and to what extent increases in stimulus-onset triggered averages can be attributed to eye muscle contamination. In general the answer is expected to depend on the task and the number of repetitions, as well as the presence and magnitude of any cortical responses, in addition to the magnitude of oEMG contamination. All of these may affect the correlation between oEMG power and factors of interest in the experimental design. For the current visual search task, numerous channels show significant (FDR q-value = 0.01) modulation of the power in the gamma range following stimulus onset (Fig. 10) in the

Common   Bipolar

No ICA

1 IC

2 IC

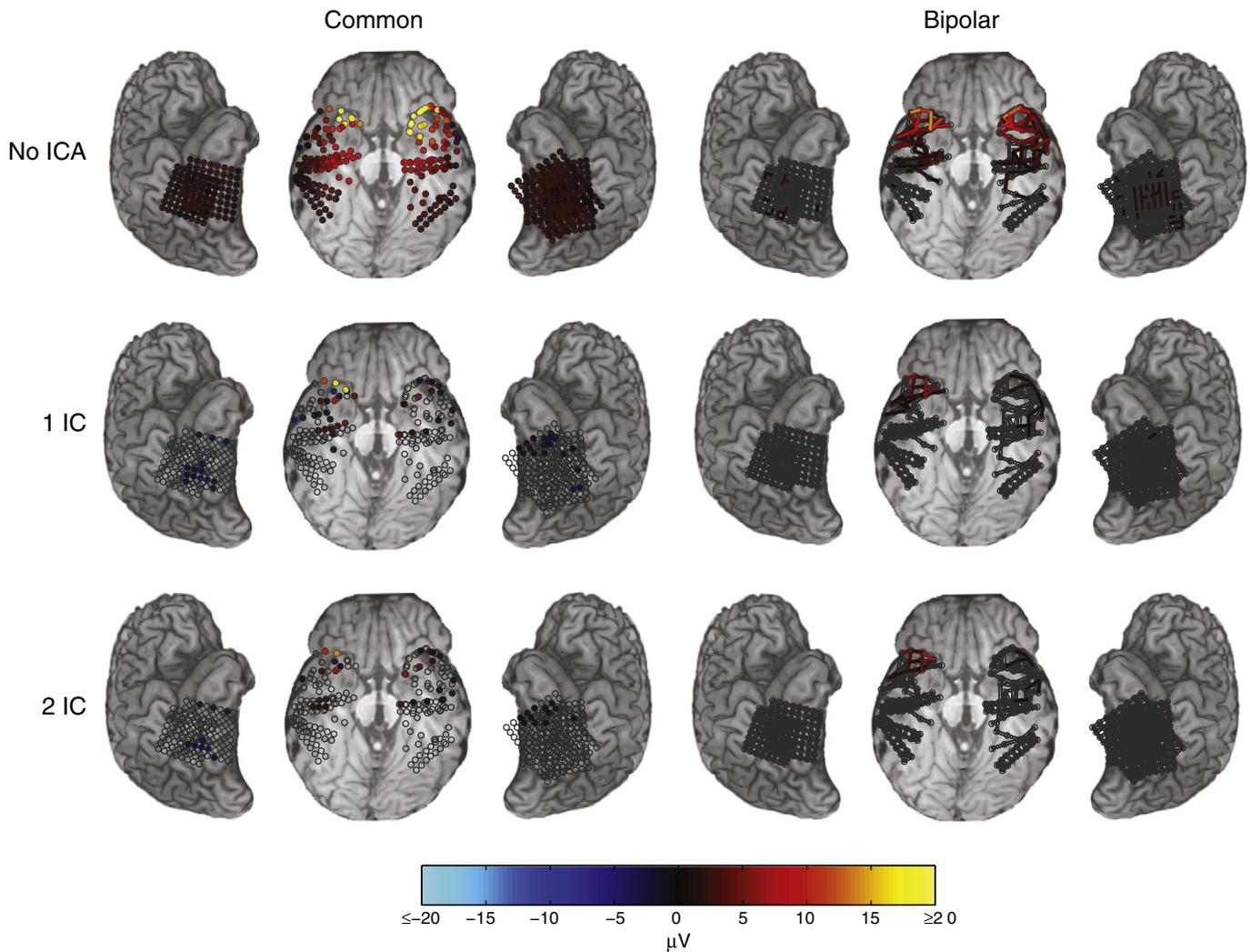≤−20   −15   −10   −5   0   5   10   15   ≥2 0

μV

Fig. 9. Effect of ICA filtering (rows) and bipolar rereferencing (columns) on iSSP peak-to-trough amplitude. Data in the left column are in the original common reference space. In the right column, data have been rereferenced to neighboring contacts within at most 1 cm, indicated by elongated bars. The top row shows amplitude without ICA filtering, the second row after removing the first sorted independent component, and the third row after removing the first and second sorted independent component. Contacts for which the response does not reach significance threshold of FDR $q = 0.01$ are unfilled.

positive direction (56, 26, 57, 52 and 36 contacts out of 128 respectively for subjects 1 to 5), and in each case a smaller number showed significant reduction of gamma power (11, 19, 2, 10 and 3 contacts, respectively). Channels in which there is a large iSSP show a saccade onset-following response in the trial average, which is suppressed by ICA filtering (Figs. 10 and 12), establishing that the response in the trial average is related to eye movement contamination. In the posterior contact PVT, a large response at the trial onset is not associated with any saccade onset response (Row 3, Fig. 13), and is not affected by ICA filtering. Thus the response in PVT cannot be attributed to oEMG contamination. Interestingly, PVT does show a post-saccadic modulation characterized by suppression of the gamma response followed by enhancement, a pattern which resembles saccade related modulation of multiunit activity (Rajkai et al., 2007; Ringo et al., 1994).

To show the contribution of contamination across all channels, the 70–100 Hz band was chosen for further analysis as a representative bandwidth within the range of observed broad-band gamma modulation, which avoided 60 and 120 Hz bands likely to be affected by line noise. Mean 70–100 Hz log power was computed within the window 0–500 ms following trial onset. Significant elevation of power above the baseline is suppressed by ICA filtering within this window in channels clustered over the anterior half of the ventral temporal surface

(Fig. 10C). The contribution of the filtered components to power within the window is large (~1 dB) over the anterior third and declines rapidly to less than 0.5 dB within the middle third (Fig. 10D). Over the posterior third the effect is negligible. In total, channels which showed a significant increase in gamma power before ICA filtering but not afterward numbered 8, 9, 22, 15 and 14 out of 128, respectively, for the five subjects. A total of 4 channels, 3 for subject 2 and 1 for subject 1, showed a significant response after filtering, but not before. Channels in which the response was significant both before and after filtering numbered 67, 28, 37, 47, and 25, respectively.

Comparison of oEMG and visual response

As noted, numerous contacts showed increases in gamma-band power which was not attributed to eye muscle contamination. The comparison of responses in PVT and the contaminated signal in TP (Fig. 14A) reveals an instance of surprising similarity in the time-course and the magnitude of the two responses, especially with respect to the onset peak. Fig. 10B shows the data from TP and PVT sorted with respect to the delay between trial onset and the first saccade, revealing again that the response in TP is strongly time-locked to the occurrence of saccades. The response in PVT, in contrast, shows no sensitivity to the timing of saccades. Although the two responses are otherwise easily
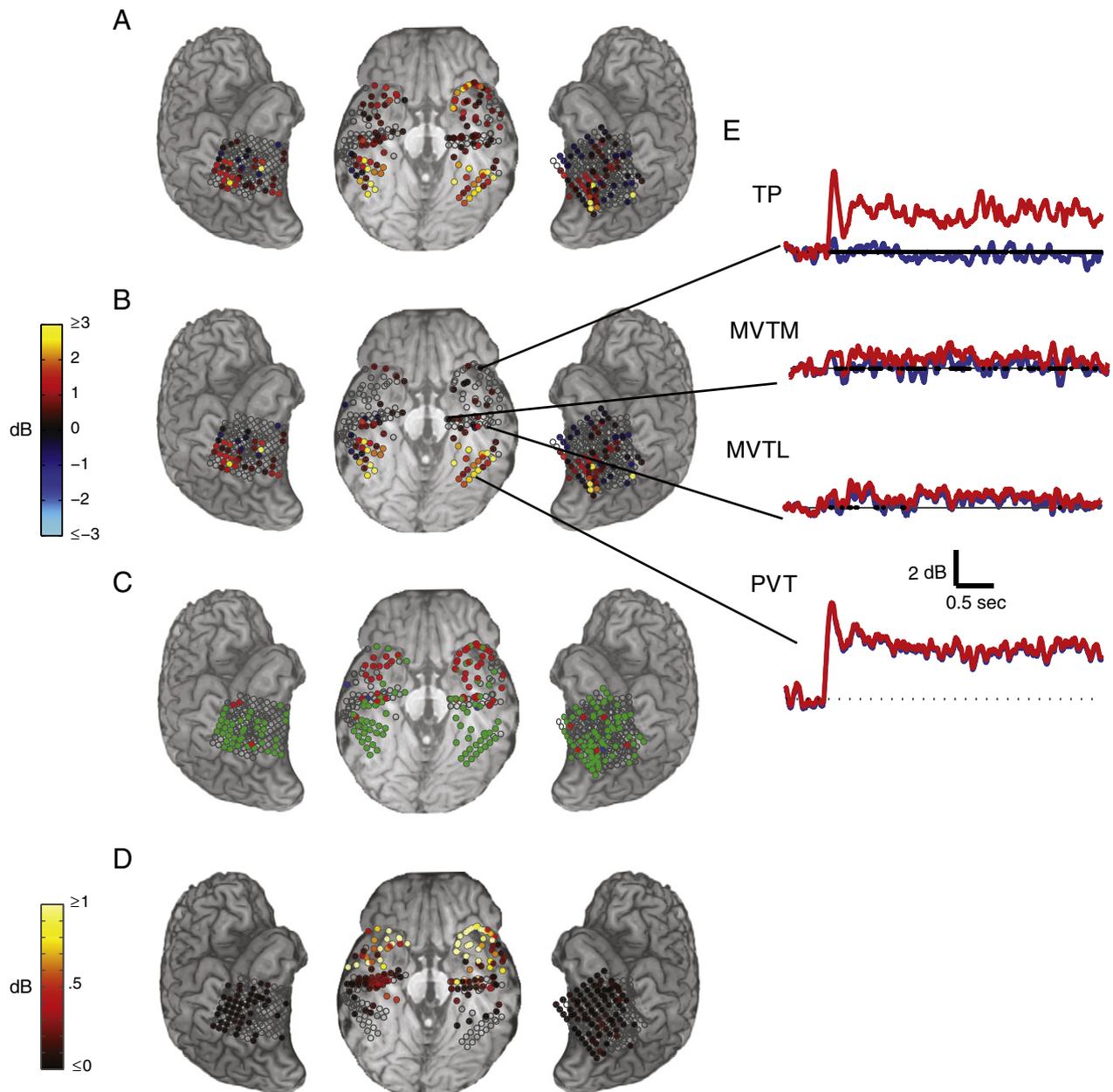
Fig. 10. Contribution of the filtered components to trial onset related 70–100 Hz band response. (A) Mean log band power increase (dB) in the 0–500 ms epoch after stimulus onset, normalized to the −400 to −100 ms epoch. Channels for which significance did not reach a threshold of FDR $q = 0.01$ are unfilled. (B) Response after ICA filtering. (C) Summary of significance tests in A and B: contacts are colored green if the response remains significant (FDR $q = 0.01$) before and after filtering, red if the response is significant only before filtering but not after, and blue if the response is significant after filtering but not before. (D) Contribution of filtered independent components to trial onset response log power, measured as the decibel log-ratio of power in the 0–500 ms epoch between ICA filtered and unfiltering data. (E) Average log band power for the entire duration of the trial in selected channels, before ICA filtering (red) and after filtering (blue). Selected channels are from temporal pole (TP), mesial ventral temporal cortex, middle section (MVTM), lateral ventral temporal cortex, middle section (MVTL) and posterior ventral temporal cortex (PVT). Time points when the difference between the unfiltered and filtered response is significant (FDR $q = 0.01$) are shown by thick black line segments along the x-axis.

distinguished from each other on the basis of anatomical separation, they cannot be reliably distinguished from each other on the basis of time course in the trial average. As seen in Fig. 12 the responses also share a similar bandwidth, thus spectral features and time-course of the responses provide no obvious gross attributes by which to distinguish oEMG contamination from neuronal signal. Some subtler differences are apparent, however: in the case of oEMG in TP contamination the initial peak is followed by a trough, which reflects a decrease in saccade frequency following the initial peak, related to the duration of the succeeding fixation. This trough is not present in the visual response in PVT. The spectrum of oEMG contamination also extends into a lower frequency range, to approximately 20 Hz, whereas the response in PVT is confined to frequencies above 40 Hz and is accompanied by

suppression of lower frequencies. These differences might be used to distinguish oEMG contamination from cortical gamma-band responses in some cases, although we cannot establish how reliably these features accompany the respective signals. The possibility that the observed response may be a mixture of oEMG and cortical sources is likely to further limit their usefulness.

Coherence

Measures based on cross-spectral power, such as coherence, may be especially susceptible to the effects of contamination when compared locations are affected by volume conduction from a common source. We therefore examined saccade-onset-related changes in interchannel

coherence (Fig. 15). The change in the distribution of coherence between the presaccadic and saccade-onset windows at each frequency pooled across all channels and subjects provides a global summary of the frequency ranges most affected by contamination. In Fig. 15E a difference is visually apparent between 40 and 110 Hz, and is confirmed by the one-tailed rank-sum test on the equality of medians, indicating that median coherence in the aggregate data is greater in the saccade onset window than in the reference window with $P < 0.001$ within each frequency band from 40 to 110 Hz.

A subsequent analysis examined pair-wise coherence changes within the 70 Hz to 100 Hz range. As shown in Fig. 15A, a significant increase in coherence is centered on anterior channels near temporal pole but also extends widely over much of anterior and lateral cortex. In channels over posterior and lateral temporal cortex, significant changes in coherence involve ventral anterior and medial channels where the iSSP is greatest.

Threshold-based artifact rejection

In EEG recordings eye-movements often appear as large amplitude voltage fluctuations, which reflect contamination by the EOG signal. Such large amplitude fluctuations may be detected and discarded using simple threshold-based artifact rejection. We therefore examined the usefulness of a threshold-based procedure in detecting and removing eye movement related contamination. We compared the number of peri-saccade onset windows (−50 to 50 ms with respect to saccade onset) which contained voltages that exceeded threshold with the number of presaccadic baseline windows (−150 to −50 ms) across all saccades, during which there were few saccades. Using a 5 s.d. criterion, a difference between the windows was observed at an uncorrected P-value of 0.05 in 13 channels across all subjects, of which only 1 channel remained significant at $q = 0.05$ after applying FDR correction. This channel was a temporal pole contact for which iSSP peak-to-trough amplitude was 45.6 μV. At a lower threshold criterion of 4 s.d. the number of contacts showing a significant difference increased to 4. Thus eye-movement related artifacts either from muscle, EOG, or other sources did not create a large amplitude disturbance that could be reliably detected using a simple threshold, except in a small number of highly affected channels. In general, we did not observe that eye movements were associated with obvious large amplitude fluctuations in the unfiltered data, such as might arise from EOG contamination Thus we conclude that simple threshold-based artifact rejection is not effective for removing oEMG contamination.

Discussion

We have shown that ocular-muscle electromyogram (oEMG) contamination of intracranial recordings, particularly in the form of the iSSP, is observable throughout much of the recorded area and that contamination may affect power-spectral measurements. The iSSP closely resembles the saccadic spike as described in scalp recordings with respect to waveform and in its dependence on saccade amplitude and direction (Becker et al., 1972). The spatial gradient of iSSP amplitude apparent in Figs. 3 and 4 suggests a source near and slightly beyond the temporal pole. On depolarization, the extraocular muscles generate a dipole moment that is grossly aligned with the extraocular muscles (Thickbroom and Mastaglia, 1985; Yuval-Greenberg et al., 2008). As anterior medial contacts lie nearer to the expected axis of this dipole, the medial to lateral gradient apparent in Figs. 3 and 4 provides further evidence for an ocular-muscle source. We therefore conclude that the scalp and intracranial saccadic spike arise from a common source.

While the iSSP can be detected over a broad area covering most recorded locations, the spatial distribution of the effect on trial-onset averages of power in the gamma range is more restricted (Fig. 10), affecting mainly locations in the anterior half of temporal cortex. Large visual responses following the onset of the trial were most apparent over the posterior half, and thus did not substantially

overlap with the regions most affected by contamination. Within the middle section of ventral temporal cortex (e.g. contact MVTL, Fig. 10E), small amplitude visual responses appeared to overlap with oEMG contamination, leading to potential ambiguity in the source of the more subtle response.

We also observed that spectral characteristics and time course of eye movement contamination in contacts near temporal pole can closely resemble gamma-band visual responses recorded elsewhere in the same patients. This emphasizes the potentially seriously confounding nature of the oEMG contamination: not only can it obscure cortical activity, but it can be mistaken for it. In the present task, many contacts over posterior ventral cortex, notably near areas responsive to faces (Allison et al., 1999; Tsuchiya et al., 2008) showed large broad-band increases of power in the gamma range (exemplified by contact PVT in Figs. 10–14). We verified that these responses do not arise from oEMG contamination, and most likely therefore reflect genuine cortical activity. Like the oEMG signal, the cortical response covers much of the observed spectral range between 40 Hz and 200 Hz.

The similarity in the time course of visual responses in some channels and the oEMG signal deserves special attention. For example, the contaminated signal from contact TP and the cortical response in PVT both show a peak between 200 and 300 ms (Fig. 14), followed by a sustained elevation of gamma power over the remainder of the trial. This similarity might suggest that gamma-band activity in extrastriate visual cortex is correlated with the frequency of eye movements, a finding which has been described in the BOLD response of primary visual cortex (Kimmig et al., 2001), however the onset and initial peak within the high gamma response in PVT did not otherwise closely follow the latency to the first saccade (Fig. 14B). Moreover, in two adjacent channels, PVT−1 and PVT+1, the peak latencies were shifted backwards and forwards in time, respectively (Fig. 14A). In PVT the initial peak represents an onset response following the appearance of the stimulus; the fact that the onset of the first saccade coincided with this peak suggests that it is programmed well before this early visual response. Targeting of such rapid initial eye movements seems likely to depend rather on very early visual responses in frontal eye field (Kirchner et al., 2009), than on the output of more delayed visual processing in ventral temporal cortex.

A second observation concerns the similarity in the bandwidth of the two responses: in the case of the saccadic spike, the breadth of the spectral response is the signature of a highly transitory, weakly oscillatory (biphasic) signal. Because of variability in timing, averaging smears this response in the time direction, leading to the appearance of a more sustained activation. There are three different mechanisms that might produce a similar signature in spectral averages of the cortical signal. First, it is possible that the breadth of cortical responses in the gamma range reflects weakly oscillatory transients, similar to the oEMG signal, which vary in timing from one trial to the next. Second they might arise from sustained narrow-band oscillations whose modal frequency varies from one trial to the next, and third they might represent sustained weakly oscillatory broad-band activity which is similar across trials. Finding the proper analytical techniques to distinguish different types of temporal structure that lead to the same average spectrogram is therefore an important matter, which may prove useful for identifying oEMG contamination.

Dependence on saccade amplitude

The relationship between saccade amplitude and iSSP peak-to-trough amplitude agrees with the general relationship described in scalp recordings (Boylan and Doig, 1989): iSSP amplitude increases rapidly and approximately linearly with saccade amplitude up to 8 degrees, beyond which it approaches a stable plateau (Figs. 5, 6, 7). One consequence of the rapid increase of the saccadic spike amplitude in
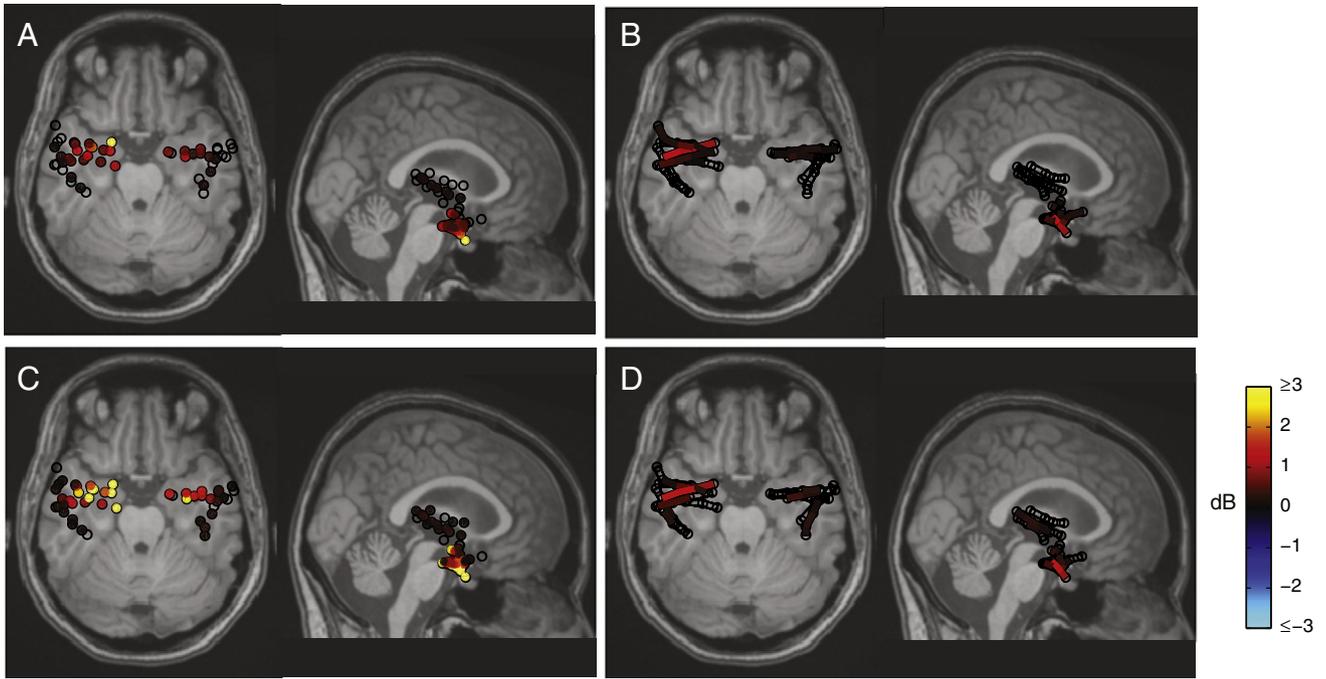
Fig. 11. Effect of ICA filtering on trial onset responses in depth recordings. The change in 70–100 Hz power following task onset, normalized to respective filtered and unfiltered baselines, is shown for the common reference (A) and after nearest-neighbor rereferencing (B). The contributions of filtered components to signal power (log ratio of power without normalizing to baselines, as in Fig. 10D) following trial onset are shown in C and D.

scalp recordings is that small amplitude saccades may generate non-negligible contamination (Keren et al., 2010; Yuval-Greenberg et al., 2008). We observed iSSPs in a few channels for saccades of less than 2 degrees, which were restricted to the anterior third of ventral temporal contacts. Given the precision of gaze position recordings, we cannot address the occurrence of intracranial oEMG during microsaccades (with amplitude less than 0.5 degrees), which cannot be eliminated with instructed fixation. Suppressing large amplitude eye movements should reduce the practical consequence of contamination in the trial-onset average, and may eliminate the problem altogether in some cases. However we cannot draw strong positive or negative conclusions on the possible role of small saccades, as the data may also be biased by the presence of false positives in saccade detection, which are most likely to be classified as small amplitude saccades. Given that the iSSP is nevertheless clearly present in some channels for saccades of less than 2 deg, we recommend that, at a minimum, recording and reference electrode locations should be considered when ruling out contamination for small amplitude saccades. A more thorough evaluation of this point will require higher precision eyetracking.

Contribution of the reference electrode

At locations distant from the temporal poles, notably posterior ventral temporal cortex and lateral temporal cortex we found contamination to be negligible in its effect on trial-onset averaged gamma power. It is therefore tempting to use proximity to the orbit as an additional criterion for ruling contamination in or out. However, it must be remembered that the signal reflects the voltage difference between recording and reference contacts, and that the absence of a signal implies that the voltage fluctuations are equal at both locations, not that that the signal is truly absent at either location, compared to a perfectly neutral ground. In particular, whether oEMG contamination might be attributed to the reference contact ("reference contamination") depends on the magnitude and polarity of the signal at both the reference and the recording sites. Because in the present case an extracranial subgaleal electrode near the vertex served as reference, an implication is that iSSP-related oEMG appears over much of

posterior and lateral recording locations with a similar polarity and magnitude as at the scalp vertex. Saccadic spike amplitude at the scalp vertex, referenced to comparatively neutral non-cephalic locations, has been reported with the same polarity that we observe in the intracranial recordings at an amplitude of approximately 15 μV (Thickbroom and Mastaglia, 1985). With respect to a hypothetical, perfectly neutral reference, our findings therefore suggest that the signal is substantial throughout the head and distributed on a scale similar to that at the scalp. Because the polarity of the iSSP at the scalp reference, relative to ground, is expected to be the same as what we observed at the large majority of intracranial locations, it is also unlikely that the choice of reference substantially increased the observed iSSP: had the reference contact introduced an upward bias in the magnitude of the observed oEMG contamination in any channels, it should have been accompanied by a widely distributed polarity reversal of the iSSP within all channels for which the reference contamination exceeded recording contact contamination. Based on the known distribution and amplitude of the scalp SSP and the orientation of equivalent source dipoles (Thickbroom and Mastaglia, 1985; Yuval-Greenberg et al., 2008), we expect that a more anterior reference would have resulted in a larger and more widely dispersed iSSP and greater contamination of spectral power in the gamma range. These conclusions must be tempered by the fact that we cannot directly infer the amplitude of the iSSP in the reference contact from the present data, and that the presence of surgical bone and tissue defects may cause scalp topography to deviate from the previously reported distribution. That the extracranial reference in the present case was the major source of contamination can be ruled out with greater confidence from the fact that the response shows a large gradient across intracranial locations near anterior temporal pole, and that the effect of contamination in the trial- and saccade-onset averages became negligible at posterior and lateral locations, where the signal is expected to be smallest. The question of the distribution of the signal might be further clarified with a detailed model of head conductivity, but it is safe to conclude that the choice of reference in intracranial recordings, as in scalp recordings, will have important consequences in the likelihood of observing contamination.
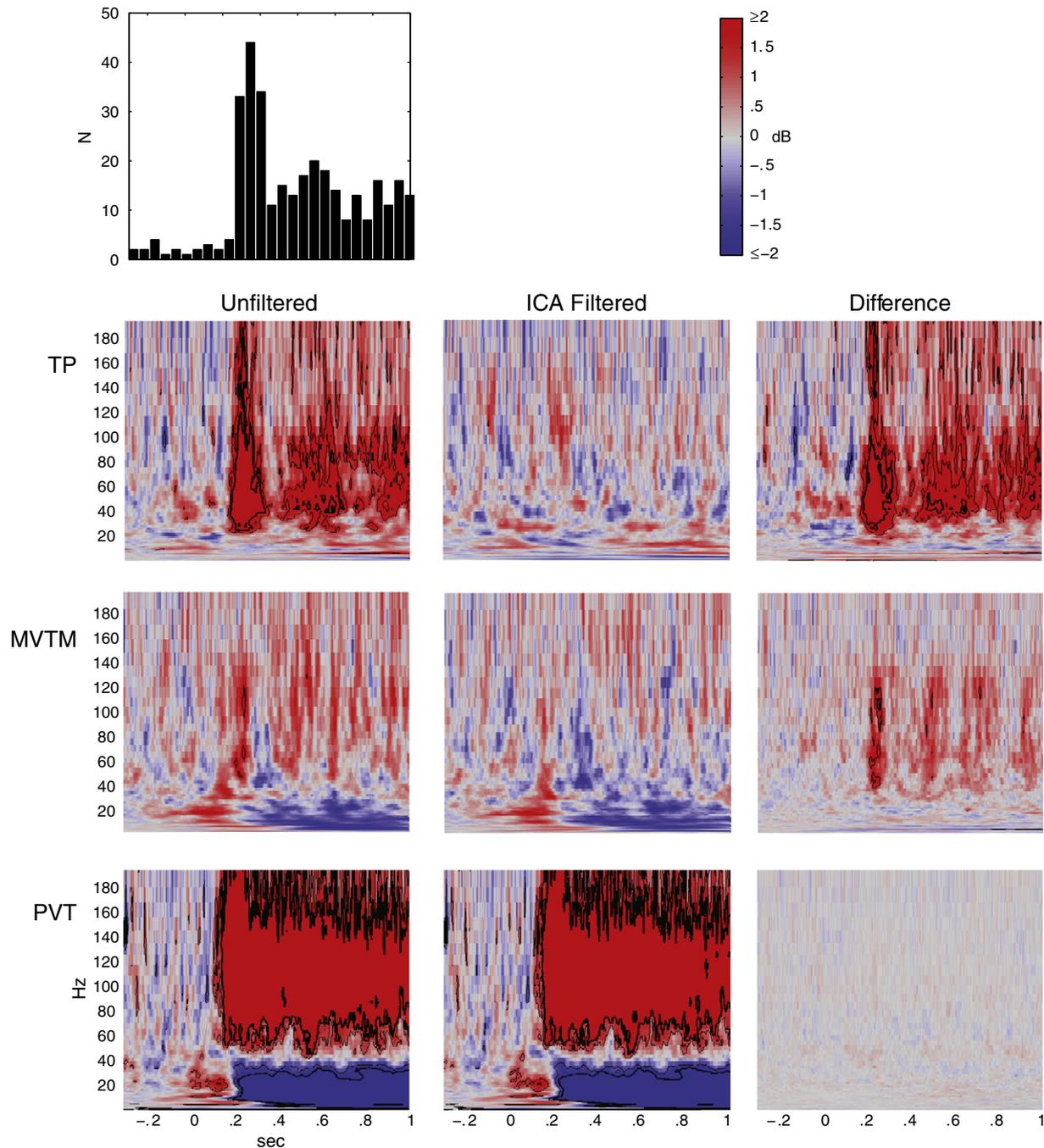
Fig. 12. Log power wavelet spectrograms showing average trial onset related spectral perturbation at temporal pole (contact TP, labeled in Fig. 10), mesial ventral temporal cortex (contact MVTM), middle section, and posterior ventral temporal cortex (PVT). Thick black lines indicate significance regions for FDR $q = 0.001$ and thin black lines for $q = 0.05$. Left column shows response before ICA filtering, middle column after filtering, and right column shows the difference of the two. The top left panel shows the histogram of saccade onsets within 50 ms bins.

Comparison to previous reports

The present findings complement recent studies which describe motor and eye-movement contamination of intracranial recordings. Of particular relevance, Jerbi and coauthors also observed the iSSP at a handful of recording contacts near the apex of the temporal pole (Jerbi et al., 2009a), which did not affect more posterior and anterior recording locations. They conclude that oEMG contamination in bipolar stereotactic EEG outside of temporal pole is likely to be negligible. We have described contamination with a considerably wider distribution, affecting both subdural ECoG and depth recordings. This difference can be accounted for by the methods of

referencing used by the respective studies. Jerbi and colleagues obtained recordings with a nearest-neighbor bipolar derivation spaced at 3 mm. Consistent with their observation, we found that offline bipolar referencing greatly suppresses the extent of contamination, though not to same the degree described by them. The spacing of bipolar pairs (3 mm) in their report was smaller than what we were able to reproduce in our analysis, as minimum inter-electrode distance varied between 1 cm and 5 mm in our recording arrays. The apparently lower effectiveness of bipolar rereferencing in the present case is likely to be a consequence of greater distance between reference and recording locations. Jerbi and colleagues also obtained recordings in the context of a reading task, which may have
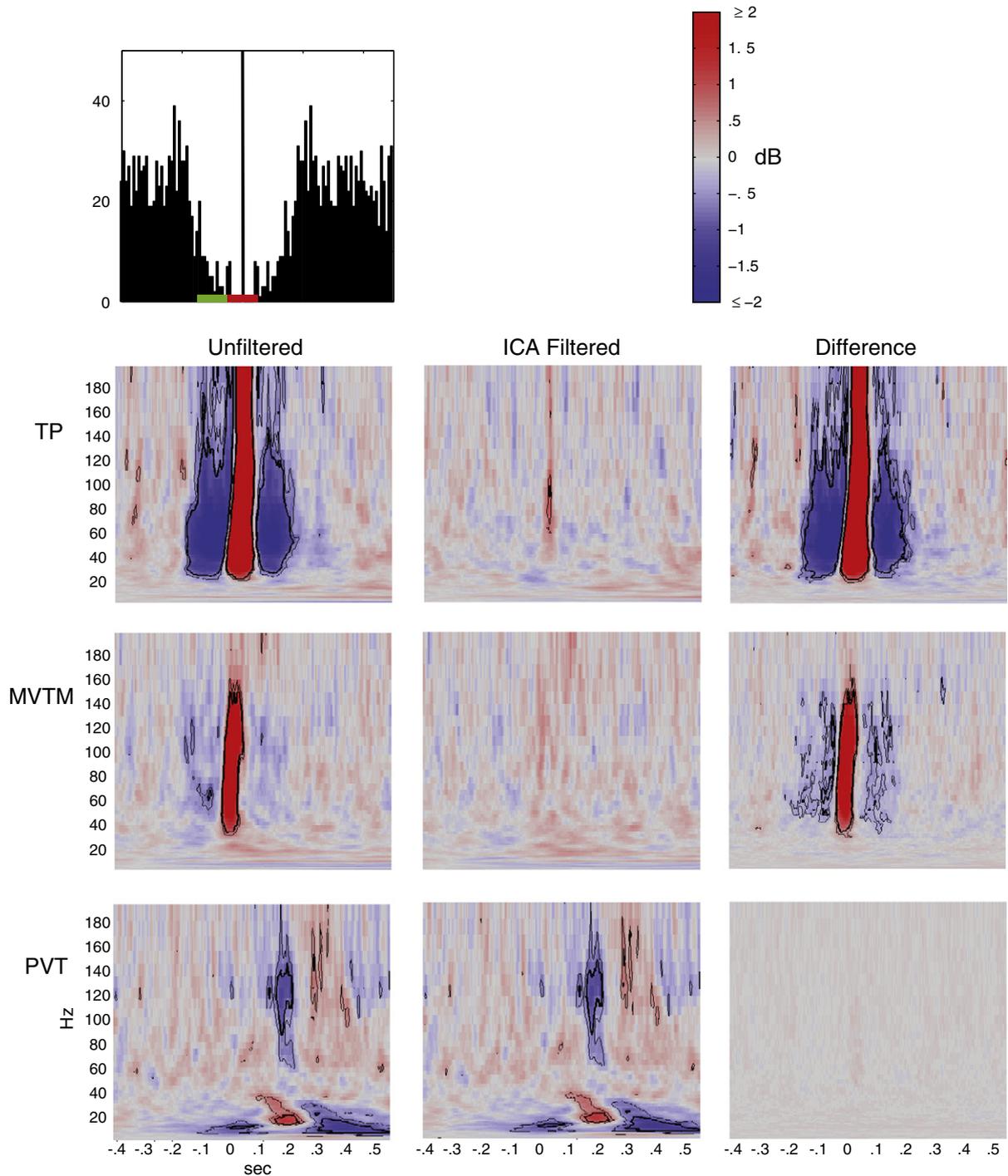
Fig. 13. Log power wavelet spectrograms showing average saccade related spectral perturbation (averaged with respect to saccade onsets detected by eye tracker) for the same contacts as in Figs. 10 and 12. Power is normalized to the −500 to −200 ms epoch preceding saccade onset. Thick black lines indicate significance regions for FDR $q = 0.001$ and thin black lines for $q = 0.05$. Left column shows response before ICA filtering, middle column after filtering, and right column shows the difference of the two. The top left panel shows the histogram of saccade onsets within 5 ms bins. The post-saccadic refractory period following the previous saccade, falling within the preceding fixation, is shown (green line), as well as the perisaccadic window (red line).

tended to favor smaller amplitude saccades than our visual search task. Finally, electrodes were implanted in the left hemisphere, while the data were collected in a reading task in which it can be assumed the large majority of saccades are rightward (contraversive with respect to electrode location), suggesting that a smaller signal was observed than if leftward (i.e., ipsiversive) and rightward saccades had been equally frequent (see Fig. 5). Our findings complement theirs in identifying the appearance of the oEMG contamination in intracranial recordings, while warranting a greater degree of caution

when considering oEMG contamination in common-reference recordings as well as when using more widely spaced bipolar pairs. Taken together, the studies emphasize the usefulness of local referencing, and in particular, closely spaced bipolar montages as used by Jerbi and colleagues.

Ball and colleagues compared the manifestation of eye-movement contamination in simultaneously recorded ECoG and extracranial EEG (Ball et al., 2009). They observed blink artifacts in ECoG recordings from prefrontal cortex, as well as smaller saccade-related artifacts. In
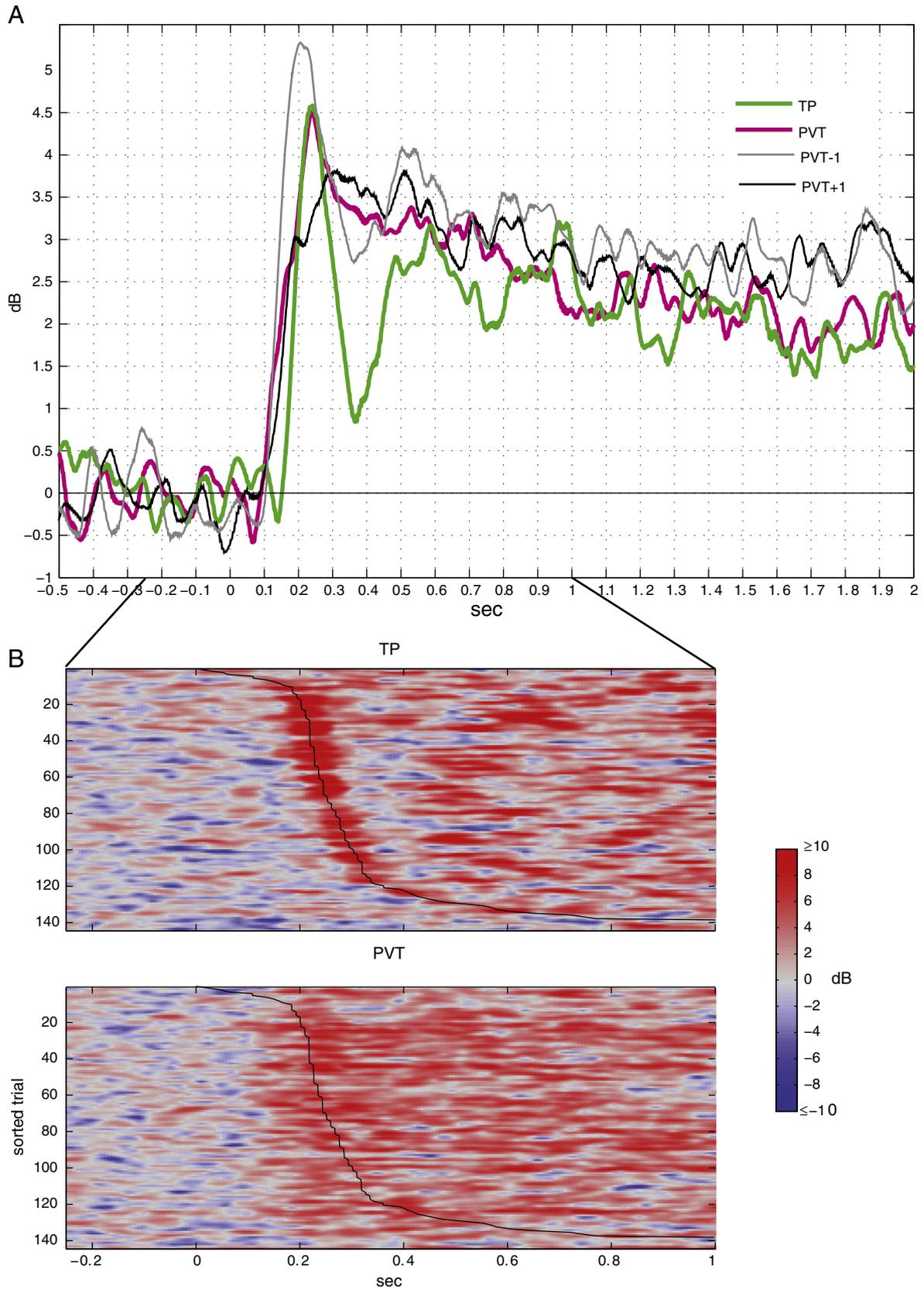
Fig. 14. An example of similarity in the time course of oEMG related responses and cortical response. Trial onset related increase in 70–100 Hz band power in the temporal pole (contact TP, green) are closely associated with eye movements, while the response observed in posterior ventral temporal contacts is not (PVT, magenta). (A) Both responses have a similar time-course including a peak at 240 ms, as well as magnitude with respect to baseline. Contacts adjacent to PVT (gray and black) also show a similar pattern, although with different amplitudes and latencies in the initial peak. (B) Sorting trials by the delay to the first saccade reveals that the response is strongly time-locked to saccade onset (black line) in TP (top) but not in PVT (bottom). The data were smoothed over trials with a five-point moving average applied after sorting.

both cases the signals resembled blink and eye-movement related components of the classical EOG signal, which arise from the corneoretinal potential and from blink-related changes in conductivity of the eye, rather than muscle depolarization (Arden et al., 1962 ; Kris, 1958; Miles, 1939). Because saccades were determined from the EOG signal, rather than direct recordings of eye movement, it is likely that alignment error would have suppressed the iSSP in the averaged signal, had it been present, thus the study does not address motor contamination of the type considered here. Ball et al. also did not report saccade related spectral perturbation, however it is noteworthy in our data that perturbation in the dominant frequency ranges of the classical EOG signal (below 20 Hz) was absent (Fig. 13). This observation suggests that oEMG-related gamma-band contamination is substantially larger within the respective frequency range, relative to the physiological background, than the contribution of components of the classical EOG identified by Ball et al. Thus the current findings suggest important differences between the manifestation of oEMG and EOG contamination and, in particular, that the appearance of one may not be a reliable predictor of the other. Methods optimized to remove EOG contamination may not reliably remove oEMG contamination, and vice versa.

The manifestation of EMG in intracranial recordings has recently been addressed in a case report by Otsubo et al. (2008), who observed widely distributed EMG signals during chewing and seizure related facial grimacing in a single patient. Of a series of 38 pediatric epilepsy patients, the reported case was the only one in which such EMG contamination was noted. Facial muscle EMG contamination therefore appears to be comparatively unusual and less consistent across subjects than oEMG contamination, which we find to be similar in all five observed subjects with respect to magnitude and distribution. Otsubo et al. suggest that facial muscle EMG contamination is likely to depend on the position of surgical bone defects relative to the recording array (Zhang et al., 2006), and therefore to vary from case to case. We find the oEMG signal, in contrast, to be consistent in its distribution and magnitude across subjects, suggesting that the normal anatomical relationship between the orbital cavity and the intracranial space, which are connected by the superior orbital fissure and optic canal, explain the current spread from one compartment to the other. Further clarification of such questions will require anatomically detailed source modeling.

Effect on interchannel coherence

The effect of contamination from a distant source is especially important to consider when measuring inter-channel coherence and related measures of coupling derived from cross spectra. We find that iSSP contamination manifested as a broadly distributed pattern of increased coherence around the onset of the saccade (Fig. 15), which was mitigated by bipolar rereferencing and ICA filtering. This observation raises a concern about the use of coherence in common-reference data. It has been suggested that reference contamination is sufficiently low to permit meaningful computation of coherence in scalp-referenced intracranial recordings (Zaveri et al., 2000). The present finding suggests that a more serious confounding factor arises from common source contamination related to oEMG, rather than reference contamination. Methods which attempt to eliminate the effect of contamination from common sources by removing zero-phase-lag coherence (Nolte et al., 2004; Stam et al., 2007) might be applicable, however because contamination in this instance arises from multiple mutually coherent sources (left and right extraocular muscles), rather than a single source, it remains possible that a portion of the change in coherence will appear with a non-zero phase lag. That left and right-sided contacts mirrored each other in their dependence on saccade direction implies that they were affected, at least in part, by different sources. This important issue requires further scrutiny, but we recommend care in ruling out muscle contamination as a source of inter-channel coupling, particularly when using a common reference.
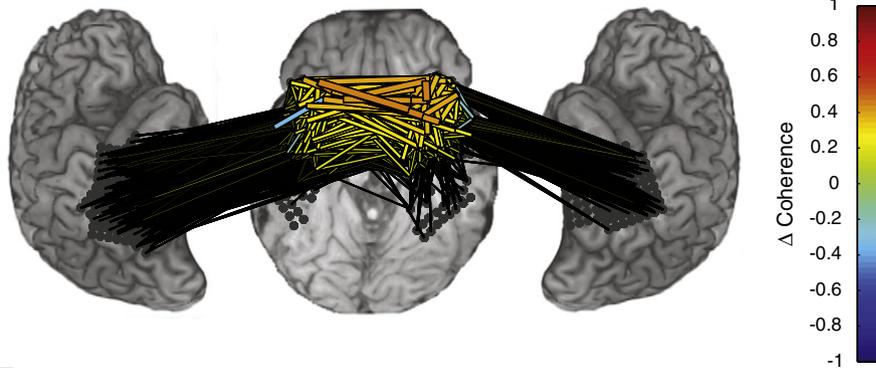
Distinguishing oEMG from cortical signals: recommendations for future studies

The current observations suggest some general guidelines for ruling out eye-movement related motor contamination in intracranial data. When eye-movement data are available, the simplest procedure is to examine spectral power averaged with respect to saccade onset. In the absence of a saccade-onset associated spectral perturbation, any stimulus-onset response is not likely to be explained by oEMG contamination. When eye-movement recordings are not available, several options remain. First, oEMG can be suppressed using spatial filtering such as local rereferencing or ICA. Local rereferencing is generally easiest to implement, and we found that it reduced the extent of the effect on gamma-band power and interchannel coherence, but left significant contamination over the portion of the recorded area where the gradient of the response was steep, roughly the anterior third of temporal cortex. ICA filtering requires the identification of components containing the muscle artifact; although we selected components on the basis of perisaccadic power, we might also have identified them from the characteristic anteroposterior gradient in the mixing coefficients (Fig. 8) and the broad-band spikes which were visible in the unaveraged data, whose occurrence followed the expected time course of eye movements. Similar criteria have recently been applied successfully to component selection in scalp EEG (Keren et al., 2010); our results suggest they are also applicable to intracranial data, provided there is adequate spatial sampling to isolate the artifact. Whereas electrode placement in scalp EEG recording is highly standardized, placement of intracranial contacts inevitably varies from one patient to the next; thus, the effectiveness of ICA filtering applied to intracranial data is less easy to predict in advance. Regression based methods provide yet another alternative (McMenamin et al., 2009; Nottage, 2010), which we have not evaluated here. Although we show that small amplitude saccades generate a measurable iSSP signal at some locations, the magnitude of the signal varies approximately linearly with saccade amplitude for saccades of less than 8 degrees, and suppressing large amplitude eye movements may therefore help further reduce contamination. All of the methods considered here are most effective when at least one recorded channel includes significant oEMG contamination, and future studies may benefit from extracranial recordings obtained near the orbits that are dedicated to extracting the eye muscle signal. For example, in checking for perisaccadic spectral perturbation, one should have one or more channels in which the oEMG signal is present to serve as a positive control, which validates the conclusion that any other channels are free of contamination. ICA is also likely to isolate the oEMG signal from neural sources more effectively when it is present in some channels with high signal to noise ratio. Especially when recording from medial or anterior temporal lobe, or when using common reference or widely spaced bipolar recordings, adding periorbital extracranial channels to capture oEMG signal is advisable. Finally, oEMG contamination varies gradually with distance from the sources, and has little variability with respect to time course from one channel to the next. Therefore, a further criterion for ruling out oEMG contamination is local heterogeneity in the gamma-band response. For example, the peak times in the responses from adjacent channels displayed in Fig. 14A are dissimilar, supporting the conclusion that they cannot be fully explained by a common contaminant.
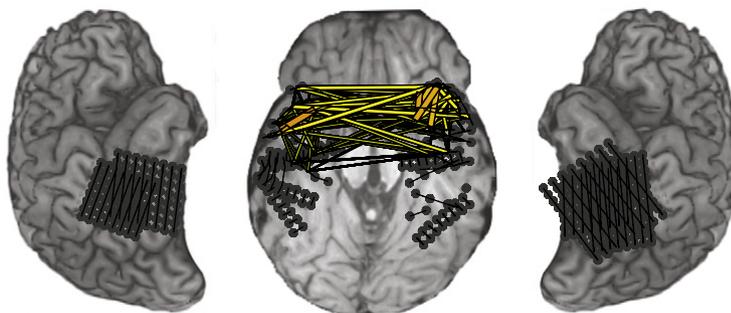
Conclusion

In summary, we find that saccade-related oEMG contamination can affect intracranial EEG obtained with a common reference in much the same way as it can scalp EEG. The assumption that intracranial recordings are more robust to oEMG contamination must therefore be qualified. However, we also note that our findings do not fundamentally overturn this assumption: in the present case the contaminating signal
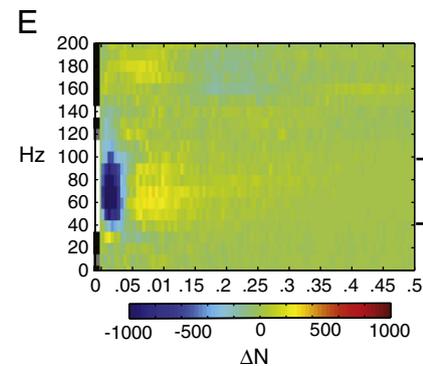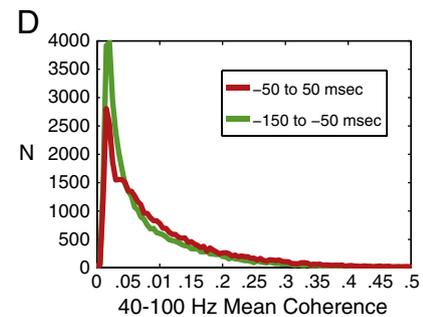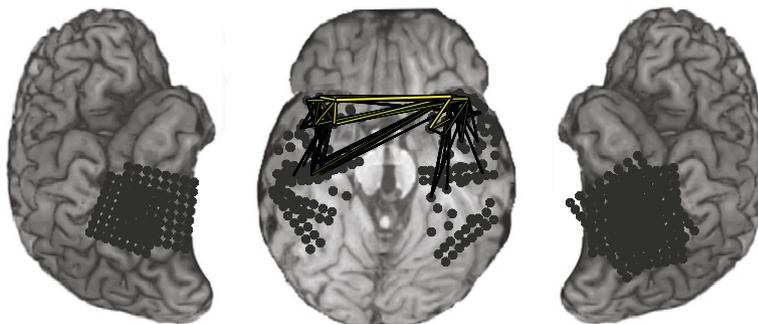
Fig. 15. Perisaccadic changes in interchannel coherence caused by oEMG contamination. Change in mean 70–100 Hz interchannel coherence between the saccade-onset window (100 ms centered at the saccade onset; red bar in Fig. 13) and a preceding reference period (preceding 100 ms; green bar in Fig. 13) in the original data (A), after bipolar rereferencing (B), and after ICA filtering (C). Saccade onset associated change in coherence pooled across all channels and subjects. (D) The histograms for mean coherence between 40 and 100 Hz in the presaccadic (green) and saccade onset (red) windows. (E) The difference between the histogram of coherences over all channels and subjects broken down by frequency. A difference is visually most apparent between 40 and 100 Hz (bracket on the right side) and is confirmed by a one tailed rank sum test on the medians. The grayscale bar at left shows the result of a one-tailed rank sum test; frequencies at which median coherence in the saccade onset window significantly exceeds that of the presaccadic window at uncorrected P<0.001 are tagged white and are tagged gray for P<0.05.

was in most instances easily distinguished from cortical activity using relatively simple procedures. Contamination which substantially affected stimulus-onset averages was confined to recording locations near anterior and anteromedial temporal cortex. Although we find that averaged cortical gamma-band responses in ECoG may at times closely resemble oEMG contamination in spectral features and time-course, the distribution of visual responses and oEMG contamination were largely non-overlapping. An important qualification of this point is its likely dependence on reference contact location. Nearest neighbor rereferencing substantially reduces the extent of contamination, although its effectiveness depends on the spacing between recording and reference contacts as well as their position and orientation relative to the local gradient in potential. In short, deciding whether oEMG contamination might affect any result requires care and judgment in evaluating all of the

parameters of the recording arrangement with particular attention to reference location. Independent component analysis offers a principled way to isolate and remove the contaminating signal in many cases, however its effectiveness is likely to depend on the number and placement of electrodes. Finally, we confirm that broad-band gamma signals observed in extrastriate visual cortex are genuinely cortical, and cannot be explained as eye-movement related contamination.

Appendix A. Supplementary data

Supplementary data to this article can be found online at doi:10.1016/j.neuroimage.2010.08.002.

References

Akaike, H., 1974. A new look at the statistical model identification. IEEE Trans. Autom. Control 19, 716–723.

Allison, T., Puce, A., Spencer, D.D., McCarthy, G., 1999. Electrophysiological studies of human face perception. I: potentials generated in occipitotemporal cortex by face and non-face stimuli. Cereb. Cortex 9, 415–430.

Arden, G., Barrada, A., Kelsey, J., 1962. New clinical test of retinal function based upon the standing potential of the eye. Br. Med. J. 46, 449.

Baillet, S., Mosher, J.C., Leahy, R.M., 2001. Electromagnetic brain mapping. Signal Process Mag. IEEE 18, 14–30.

Ball, T., Kern, M., Mutschler, I., Aertsen, A., Schulze-Bonhage, A., 2009. Signal quality of simultaneously recorded invasive and non-invasive EEG. Neuroimage 46, 708–716.

Becker, W., Hoehne, O., Iwase, K., Kornhuber, H.H., 1972. Bereitschaftspotential, prämotorische Positivierung und andere Hirnpotentiale bei sakkadischen Augenbewegungen. Vis. Res. 12, 421–436.

Bell, A.J., Sejnowski, T.J., 1995. An information-maximization approach to blind separation and blind deconvolution. Neural Comput. 7, 1129.

Benjamini, Y., Hochberg, Y., 1995. Controlling the false discovery rate: a practical and powerful approach to multiple testing. J. R. Stat. Soc. B Methodol. 57, 289–300.

Benjamini, Y., Yekutieli, D., 2001. The control of the false discovery rate in multiple testing under dependency. Ann. Statist. 29, 1165–1188.

Boylan, C., Doig, H., 1989. Effect of saccade size on presaccadic spike potential amplitude. Invest. Ophthalmol. Vis. Sci. 30, 2521–2527.

Caviness, V.S., Meyer, J., Makris, N., Kennedy, D.N., 1996. MRI-based topographic parcellation of human neocortex: an anatomically specified method with estimate of reliability. J. Cogn. Neurosci. 8, 566–587.

Delorme, A., Makeig, S., 2004. EEGLAB: an open source toolbox for analysis of single-trial EEG dynamics including independent component analysis. J. Neurosci. Meth. 134, 9–21.

Delprat, N., Escudie, B., Guillemain, P., Kronland-Martinet, R., Tchamitchian, P., Torresani, B., 1992. Asymptotic wavelet and Gabor analysis: extraction of instantaneous frequencies. IEEE Transactions on Information Theory 38, 644–664.

Engbert, R., Kliegl, R., 2002. Microsaccades uncover the orientation of covert attention. Vis. Res. 43, 1035–1045.

Engel, A.K., Moll, C.K.E., Fried, I., Ojemann, G.A., 2005. Invasive recordings from the human brain: clinical insights and beyond. Nat. Rev. Neurosci. 6, 35–47.

Evans, A.C., Collins, D.L., Mills, S.R., Brown, E.D., Kelly, R.L., Peters, T.M., 1993. 3D statistical neuroanatomical models from 305 MRI volumes. Nuclear Science Symposium and Medical Imaging Conference, 1993., 1993 IEEE Conference Record., pp. 1813-1817 vol.1813.

Fries, P., Scheeringa, R., Oostenveld, R., 2008. Finding gamma. Neuron 58, 303–305.

Howard, M.A., Volkov, I.O., Granner, M.A., Damasio, H.M., Ollendieck, M.C., Bakken, H.E., 1996. A hybrid clinical-research depth electrode for acute and chronic in vivo microelectrode recording of human brain neurons. J. Neurosurg. 84, 129–132.

Howard, M.A., Volkov, I.O., Mirsky, R., Garell, P.C., Noh, M.D., Granner, M., Damasio, H., Steinschneider, M., Reale, R.A., Hind, J.E., Brugge, J.F., 2000. Auditory cortex on the human posterior superior temporal gyrus. J. Comp. Neurol. 416, 79–92.

Hurvich, C.M., Simonoff, J.S., Tsai, C.-L., 1998. Smoothing parameter selection in nonparametric regression using an improved Akaike information criterion. J. R. Statist. Soc.: Ser. B: Statist. Method. 60, 271–293.

Hyvärinen, A., Oja, E., 2000. Independent component analysis: algorithms and applications. Neural Netw. 13, 411–430.

Jenkinson, M., Smith, S., 2001. A global optimisation method for robust affine registration of brain images. Med. Image Anal. 5, 143–156.

Jerbi, K., Freyermuth, S., Dalal, S., Kahane, P., Bertrand, O., Berthoz, A., Lachaux, J.-P., 2009a. Saccade related gamma-band activity in intracerebral EEG: dissociating neural from ocular muscle activity. Brain Topogr. 22, 18–23.

Jerbi, K., Ossandón, T., Hamamé, C.M., Senova, S., Dalal, S.S., Jung, J., Minotti, L., Bertrand, O., Berthoz, A., Kahane, P., Lachaux, Jean-Philippe, 2009b. Task-related gammaband dynamics from an intracerebral perspective: review and implications for surface EEG and MEG. Hum. Brain Mapp. 30, 1758–1771.

Jung, T., Makeig, S., Humphries, C., Lee, T., Mckeown, M., Iragui, V., Sejnowski, T., 2000a. Removing electroencephalographic artifacts by blind source separation. Psychophysiology 37, 163–178.

Jung, T.-P., Makeig, S., Westerfield, M., Townsend, J., Courchesne, E., Sejnowski, T.J., 2000b. Removal of eye activity artifacts from visual event-related potentials in normal and clinical subjects. Clin. Neurophysiol. 111, 1745–1758.

Keren, A.S., Yuval-Greenberg, S., Deouell, L.Y., 2010. Saccadic spike potentials in gamma-band EEG: characterization, detection and suppression. Neuroimage 49, 2248–2263.

Kimmig, H., Greenlee, M., Gondan, M., Schira, M., Kassubek, J., Mergner, T., 2001. Relationship between saccadic eye movements and cortical activity as measured by fMRI : quantitative and qualitative aspects. Exp. Brain Res. 141, 184–194.

Kirchner, H., Barbeau, E.J., Thorpe, S.J., Regis, J., Liegeois-Chauvel, C., 2009. Ultra-rapid sensory responses in the human frontal eye field region. J. Neurosci. 29, 7599–7606.

Kris, C., 1958. Corneo-fundal potential variations during light and dark adaptation. Nature 182, 1027–1028.

Lachaux, J.-P., Hoffmann, D., Minotti, L., Berthoz, A., Kahane, P., 2006. Intracerebral dynamics of saccade generation in the human frontal eye field and supplementary eye field. Neuroimage 30, 1302–1312.

McMenamin, B.W., Shackman, A.J., Maxwell, J.S., Greischar, L.L., Davidson, R.J., 2009. Validation of regression-based myogenic correction techniques for scalp and source-localized EEG. Psychophysiology 46, 578–592.

McMenamin, B.W., Shackman, A.J., Maxwell, J.S., Bachhuber, D.R.W., Koppenhaver, A.M., Greischar, L.L., Davidson, R.J., 2010. Validation of ICA-based myogenic artifact correction for scalp and source-localized EEG. Neuroimage 49, 2416–2432.

Meador, K.J., Ray, P.G., Echauz, J.R., Loring, D.W., Vachtsevanos, G.J., 2002. Gamma coherence and conscious perception. Neurology 59, 847–854.

Miles, W., 1939. The steady polarity potential of the human eye. Proc. Natl Acad. Sci. USA 25, 25.

Nolte, G., Bai, O., Wheaton, L., Mari, Z., Vorbach, S., Hallett, M., 2004. Identifying true brain interaction from EEG data using the imaginary part of coherency. Clin. Neurophysiol. 115, 2292–2307.

Nottage, J., 2010. Uncovering gamma in visual tasks. Brain Topogr. 23, 58–71.

Otsubo, H., Ochi, A., Imai, K., Akiyama, T., Fujimoto, A., Go, C., Dirks, P., Donner, E.J., 2008. High-frequency oscillations of ictal muscle activity and epileptogenic discharges on intracranial EEG in a temporal lobe epilepsy patient. Clin. Neurophysiol. 119, 862–868.

Rajkai, C., Lakatos, P., Chen, C.-M., Pincze, Z., Karmos, G., Schroeder, C.E., 2007. Transient cortical excitation at the onset of visual fixation: Cereb. Cortex, bhm046.

Reva, N.V., Aftanas, L.I., 2004. The coincidence between late non-phase-locked gamma synchronization response and saccadic eye movements. Int. J. Psychophysiol. 51, 215–222.

Riemslag, F.C., Van der Heijde, G.L., Van Dongen, M.M., Ottenhoff, F., 1988. On the origin of the presaccadic spike potential. Electroencephalogr. Clin. Neurophysiol. 70, 281–287.

Ringo, J.L., Sobotka, S., Diltz, M.D., Bunce, C.M., 1994. Eye movements modulate activity in hippocampal, parahippocampal, and inferotemporal neurons. J. Neurophysiol. 71, 1285–1288.

Smith, S.M., Jenkinson, M., Woolrich, M.W., Beckmann, C.F., Behrens, T.E.J., Johansen-Berg, H., Bannister, P.R., De Luca, M., Drobnjak, I., Flitney, D.E., Niazy, R.K., Saunders, J., Vickers, J., Zhang, Y., De Stefano, N., Brady, J.M., Matthews, P.M., 2004. Advances in functional and structural MR image analysis and implementation as FSL. Neuroimage 23, S208–S219.

Stam, C.J., Nolte, G., Daffertshofer, A., 2007. Phase lag index: assessment of functional connectivity from multi channel EEG and MEG with diminished bias from common sources. Hum. Brain Mapp. 28, 1178–1193.

Thickbroom, G.W., Mastaglia, F.L., 1985. Presaccadic "spike" potential: investigation of topography and source. Brain Res. 339, 271–280.

Thickbroom, G.W., Mastaglia, F.L., 1986. Presaccadic spike potential. Relation to eye movement direction. Electroencephalogr. Clin. Neurophysiol. 64, 211–214.

Thomson, D., 1982. Spectrum estimation and harmonic analysis. Proc. IEEE 70, 1055–1096.

Trujillo, L.T., Peterson, M.A., Kaszniak, A.W., Allen, J.J., 2005. EEG phase synchrony differences across visual perception conditions may depend on recording and analysis methods. Clin. Neurophysiol. 116, 172–189.

Tsuchiya, N., Kawasaki, H., Oya, H., Howard III, M.A., Adolphs, R., 2008. Decoding face information in time, frequency and space from direct intracranial recordings of the human brain. PLoS ONE 3, e3892.

Yuval-Greenberg, S., Tomer, O., Keren, A.S., Nelken, I., Deouell, L.Y., 2008. Transient induced gamma-band response in EEG as a manifestation of miniature saccades. Neuron 58, 429–441.

Zaveri, H.P., Duckrow, R.B., Spencer, S.S., 2000. The effect of a scalp reference signal on coherence measurements of intracranial electroencephalograms. Clin. Neurophysiol. 111, 1293–1299.

Zhang, Y., Ding, L., van Drongelen, W., Hecox, K., Frim, D.M., He, B., 2006. A cortical potential imaging study from simultaneous extra- and intracranial electrical recordings by means of the finite element method. Neuroimage 31, 1513–1524.